Contrib Mineral Petrol (2000) 140: 55–72

Matthew L. Gorring · Suzanne M. Kay

Carbonatite metasomatized peridotite xenoliths from southern Patagonia: implications for lithospheric processes and Neogene plateau magmatism

Received: 26 January 2000 / Accepted: 1 March 2000

Abstract The mineral chemistry, major and trace element, and Sr–Nd isotopic composition of Cr-diopside, spinel peridotite xenoliths from the Estancia Lote 17 locality in southern Patagonia document a strong carbonatitic metasomatism of the backarc continental lithosphere. The Lote 17 peridotite xenolith suite consists of hydrous spinel lherzolite, wehrlite, and olivine websterite, and anhydrous harzburgite and lherzolite. Two-pyroxene thermometry indicates equilibration temperatures ranging from 870 to 1015 °C and the lack of plagioclase or garnet suggests the xenoliths originated from between ~40 and 60 km depth. All of the xenoliths are LILE- and LREE-enriched, but have relatively low $^{87}Sr/^{86}Sr$ (0.70294 to 0.70342) and high ε_{Nd} (+3.0 to +6.6), indicating recent trace element enrichment (~25 Ma, based on the low $^{87}Sr/^{86}Sr$ and high Rb concentrations of phlogopite separates) in the long-term, melt-depleted Patagonian lithosphere. Lote 17 peridotite xenoliths are divided into two basic groups. Group 1 xenoliths consist of fertile peridotites that contain hydrous phases (amphibole ± phlogopite ± apatite). Group 1 xenoliths are further subdivided into three groups (a, b, and c) based on distinctive textures and whole-rock chemistry. Group 1 xenolith mineralogy and chemistry are consistent with a complex metasomatic history involving variable extents of recent carbonatite metasomatism (high Ca/Al, Nb/La, Zr/Hf, low Ti/Eu) that has overprinted earlier metasomatic events. Group 2 xenoliths consist of infertile, anhydrous harzburgites and record cryptic metasomatism that is attributed to CO_2-rich fluids liberated from Group 1 carbonatite metasomatic reactions. Extremely variable incompatible trace element ratios and depleted Sr–Nd isotopic compositions of Lote 17 peridotite xenoliths indicate that the continental lithosphere was neither the primary source nor an enriched lithospheric contaminant for Neogene Patagonian plateau lavas. Neogene plateau magmatism associated with formation of asthenospheric slab windows may have triggered this occurrence of "intraplate-type" carbonatite metasomatism in an active continental backarc setting.

M. L. Gorring(✉)[1] · S. M. Kay
Department of Geological Sciences, Cornell University, Ithaca, New York 14853, USA

Present address:
[1] Department of Earth and Environmental Studies, Montclair State University, Upper Montclair, New Jersey 07043, USA,
e-mail: Gorringm@mail.montclair.edu,
Tel.: +1-973-6555409; Fax: +1-973-6557047

Editorial responsibility: E. H. Hauri

Introduction

Recent studies have demonstrated the importance of both carbonatite- (Yaxley et al. 1991; Dautria et al. 1992; Hauri et al. 1993; Rudnick et al. 1993; Ionov et al. 1994) and adakite- (Kepezhinskas et al. 1995, 1996; Schiano et al. 1995; Kilian 1995) metasomatized peridotite xenoliths in mafic lavas for providing information about lithospheric mantle processes and chemistry. Carbonatitic metasomatism is associated with carbonatite magmas that are thought to represent melting of mantle carbonate (Green and Wallace 1988) or are immiscible liquids exsolved from alkaline, CO_2-rich silicate magmas (Hamilton et al. 1979). Carbonatitic metasomatism is characterized by high whole-rock Ca/Al, Zr/Hf, Nb/Ta, and very low Ti/Eu ratios in mantle xenoliths. Carbonatite metasomatized peridotite xenoliths are dominantly found in intraplate settings (Tanzania, Rudnick et al. 1993; Samoa, Hauri et al. 1993); however, rare occurrences have recently been documented in the backarc of active margins where old oceanic lithosphere is subducting (southern Kamchatka, Kepezhinskas and Defant 1996). In contrast, adakitic metasomatism is associated with adakite magmas (Drummond and Defant 1990), which are melts of broadly dacitic composition that represent small-percentage partial melts of subducted oceanic crust (Kay

1978). Adakitic metasomatism is characterized by high Na, Al, Sr/Y, and low Y, Yb, in mantle xenoliths and is commonly found only in active arc regions where young (<20 Ma) oceanic crust is presently subducting (i.e., southern Patagonia, Kilian 1995) or where subduction has recently ceased (northern Kamchatka, Kepezhinskas et al. 1995, 1996).

We have collected a suite of 20 peridotite xenoliths from the Estancia Lote 17 locality in southern Patagonia (48.5°S, 70.2°W; Fig. 1) that record strong carbonatite metasomatism of the backarc mantle lithosphere. Lote 17 peridotite xenoliths are texturally and chemically similar to other carbonatite metasomatized xenolith suites from continental intraplate settings (e.g., Yaxley et al. 1991; Dautria et al. 1992; Rudnick et al. 1993). The Lote 17 xenolith suite consists of a variety of anhydrous and hydrous (amphibole ± phlogopite ± apatite) spinel peridotites that display four distinct metasomatic styles. In this paper, we report on petrographic, whole-rock and mineral, and Sr–Nd isotope compositions for ten representative Lote 17 peridotite xenoliths in order to constrain metasomatic processes in backarc continental lithosphere and to assess the role of the lithosphere and asthenosphere in the petrogenesis of Neogene Patagonian plateau lavas.

Fig. 1 Location map showing mantle xenolith occurrences, tectonic setting, and distribution of Neogene plateau lavas of southern Patagonia (*black*, Panza and Nullo 1994). Cerro Pampa location from Kay et al. (1993). Southern Volcanic Zone (*SVZ*) and Austral Volcanic Zone (*AVZ*) (*black triangles*) are from Stern et al. (1990). Xenolith localities include Estancia Lote 17, Pali–Aike (Stern et al. 1989), and Cerro del Fraile (Muñoz 1981; Kilian 1995), Tres Lagos (Ramos et al. 1982), Meseta Buenos Aires (Niemeyer 1978), and La Laurita (Ramos et al. 1982). Timing of ridge collisions are shown between fracture zones on the Antarctic Plate (Cande and Leslie 1986; Gorring et al. 1997)

Geologic setting

Several peridotite xenolith localities are known in southern Patagonia (Ramos et al. 1982; Fig. 1). The three best characterized sites are the Estancia Lote 17 (48.5°S), Cerro del Fraile (50.5°S; Kilian 1995), and the Pali–Aike localities (52°S; Stern et al. 1989, 1999). The Estancia Lote 17 locality lies within the basaltic plateau known as the Meseta Central. The site is located in the southwestern corner of the Deseado Massif and is ~250 km behind the northernmost Austral Volcanic Zone (AVZ) centers (Fig. 1). Lithosphere beneath the Deseado Massif is thought to be as old as ~1100 Ma (Pankhurst et al. 1994). This is considerably older than late Proterozoic (~650 Ma) and mid-Paleozoic

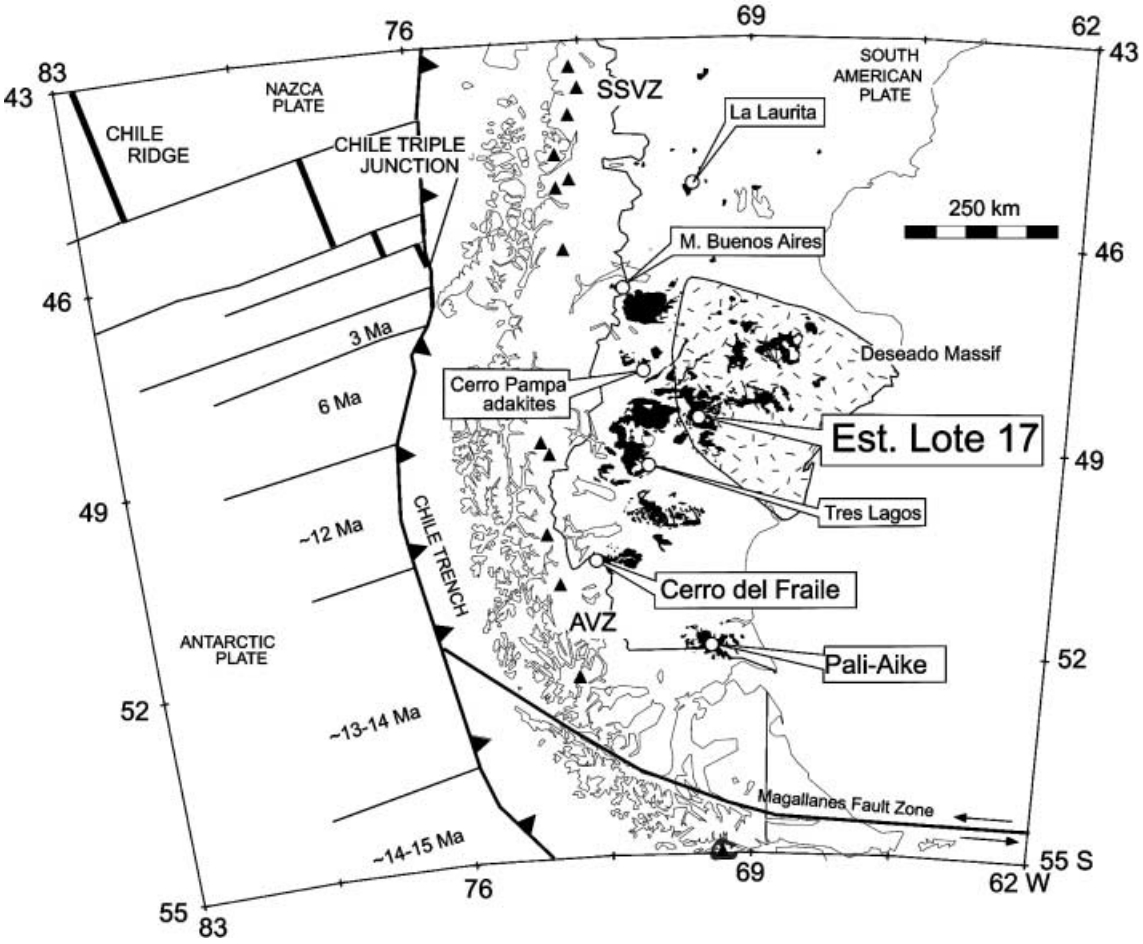

(~300 Ma) basement ages inferred to exist beneath the Pali–Aike (Ramos 1988) and Cerro del Fraile (Hervé 1988) regions, respectively.

The major tectonic/magmatic events affecting the evolution of the Patagonian lithosphere include: (1) nearly continuous subduction since the early Cretaceous and episodically since the mid-Paleozoic (Ramos et al. 1982), (2) the eruption of large volumes of Jurassic rhyolite magmatism during the incipient stages of South Atlantic rifting (Kay et al. 1989; Pankhurst and Rapela 1995), and (3) extensive Eocene and Neogene backarc plateau magmatism (Ramos and Kay 1992; Gorring et al. 1997; Gorring and Kay 2000). The Late Cenozoic tectonics have been dominated by near-orthogonal subduction of the Nazca Plate (Cande and Leslie 1986). In the Lote 17 region, Neogene plateau magmatism occurred in response to a series of Neogene ridge collisions and the opening of asthenospheric slab windows between the subducting Nazca and Antarctic Plates (Gorring et al. 1997; Gorring and Kay 2000). Two eruptive sequences are recognized: a voluminous, tholeiitic "main-plateau" sequence of late Miocene age (~10-8 Ma), and a less-voluminous, alkaline "post-plateau" sequence of Pliocene age (~3.5 Ma) (Gorring et al. 1997; Gorring and Kay 2000). Lote 17 xenoliths were entrained in a basanitic surge deposit in the post-plateau sequence.

Analytical methods

Samples were sawn into 1-cm-thick slabs. Fresh, interior sections of slabs were broken into pieces and crushed in a hardened steel mortar, then ground in a boron carbide mortar and pestle. Clinopyroxene and phlogopite separates were hand-picked under binocular microscope from the 0.5–1 mm size fraction, leached in cold 6 N HCl (cpx) or 10% acetic acid (phlog) for 30 min, and hand-picked again. Final separates were acid leached for 15 min and ground in boron carbide for trace element analysis. Unground separates were dissolved for Sr–Nd isotope analysis.

Major elements in whole rocks and minerals were determined by electron microprobe analysis (WDS) at Cornell University using a JEOL-733 Superprobe. Techniques and standards used for microprobe major element analyses are in Kay et al. (1987). Glasses were prepared from peridotite xenoliths for whole-rock major element analyses by fluxing 0.5 g of sample powder with 0.5 g of lithium tetraborate and fusing in graphite crucibles at ~1000 °C. Analyses were carried out on a JEOL-733 Superprobe in WDS mode with a 15 kV accelerating voltage, 15 nA beam current, 40 s count time, and a beam diameter of ~2 μm for minerals and 30 μm for whole-rock glasses. Whole-rock analyses represent the mean of four to six spot analyses; mineral compositions are means of one to two analyses of four to six different grains. Whole-rock analyses for TiO_2 and P_2O_5 were obtained by counting for 200 s and calibrated against glasses made from USGS standards. Typical 2σ-precision for microprobe analyses are ±1–5% for elements at >1 wt% and ±10–20% at <1 wt% concentration levels, based on replicate analysis of glass and mineral standards.

Trace element concentrations were determined by INAA and ICP-MS at Cornell University. Techniques and standards are given in Kay et al. (1987), Cheatham et al. (1993), and White and Duncan (1996). INAA and ICP-MS analyses agree within analytical error. Total analytical blanks were subtracted from all analyses and were typically <5–10% of the concentration in the most depleted harzburgite xenoliths. INAA were performed on ~0.5 g of whole-rock and ~0.3 g of mineral separate powders. Samples and standards were counted on a Ortec GeLi-detector and were counted for 24 h each to improve in-run statistics. INAA precision (2σ) based on replicate analyses of an internal basalt standard was ±5% for all elements in peridotite xenoliths, except for U, Sr, and Nd, which were ±10%. INAA precision is estimated at ±10–20% for all elements in depleted harzburgite xenoliths, except U, Th, Nd, Lu, and Sr, which were below practical detection limits. ICP-MS analyses were carried out on a VG PlasmaQuad PQ2+. Approximately 250 mg of whole-rock and 80 mg of mineral separate powders were dissolved in ultrapure, concentrated HF–HNO_3. Spinel resisted all acid attacks. Excellent correspondence between INAA and ICP-MS analyses, particularly for the HFSE, indicates that spinel did not contribute significantly to the total incompatible trace element budget of the xenoliths (e.g., Eggins et al. 1998). ICP-MS precision (2σ), based on replicate analyses of BIR and an internal basalt standard, was ±5% for LREE, HFSE, Sr, Ba, and Rb, and ±10% for HREE, U, Th, Pb, and Cs. ICP-MS precision for depleted harzburgite xenoliths is estimated at ±10–20% for all elements.

Sr and Nd isotopes were analyzed at Cornell University on a multi-collector VG Sector 54 TIMS. Chemistry and analytical techniques are from White and Duncan (1996). Approximately 250 mg of whole-rock xenolith powder and unground mineral separates were leached in hot 6 N HCl for 15 min (cold 10% acetic acid for phlogopite separates) and then dissolved in sealed 15 ml Savillex capsules with HF–HCl–HNO_3 acid mixtures. Sr and REE were separated using cation exchange columns with AG50W-x12 resin and 2.5 N and 6 N HCl as eluants. Neodymium was eluted using organically coated PFTE cation exchange resin and 0.16 N HCl. Total procedural blanks for Sr and Nd were less <100 pg, and thus negligible. No blank corrections were made.

Petrography

Lote 17 peridotite xenoliths are incompatible trace element-enriched, Type 1B, Cr-diopside peridotites (Frey and Green 1978; Wilshire et al. 1988). The collected suite consists of 20 samples of anhydrous harzburgite and lherzolite (8 samples) and hydrous (amphibole ± phlogopite ± apatite) spinel lherzolite (6 samples), wehrlite (4 samples), and olivine websterite (2 samples). The hydrous types are most likely over-represented because samples were obtained to maximize the textural and mineralogic diversity of the collected suite. Table 1 summarizes the main petrographic and mineralogic features of ten Lote 17 xenolith samples analyzed for this paper.

The xenoliths average ~10 cm in diameter and are very fresh. Textures range from coarse-grained (~3–6 mm) protogranular to medium-grained (~1–3 mm) porphyroclastic. Olivine and orthopyroxene occur as large, subhedral grains. Clinopyroxene occurs as small to large, anhedral–subhedral, bottle-green Cr-diopside. In most samples, clinopyroxene has spongy, jadeite-poor rims that are best developed in contact with olivine. Minor phases include Cr-spinel, amphibole, phlogopite, apatite, glass, and carbonate. Hydrous xenoliths contain amphibole ± phlogopite and, thus, are modally metasomatized peridotites (Dawson 1984). Hydrous xenoliths typically contain light brown, silicate glass in small (~1 mm) melt pockets and thin, grain-boundary veinlets. The glass is vesicular and some vesicles are filled with secondary carbonate.

Table 1 Summary of petrography and mineralogy of Lote 17 peridotite xenolith groups. Fo# (ol) = [Mg/(Mg + Ca + Fe)]*100; Mg# (sp) = [Mg/(Mg + Fe^{2+})] × 100; Cr# (sp) = [Cr/(Cr + Al)] × 100 where Fe, Fe^{2+}, Ca, Mg, Cr, and Al are cation proportions. Fe^{2+} by charge balance (Lindsley 1983). r^2 = sum of the square of the residuals between the calculated element analyses and the measured analyses. *lherz* lherzolite; *ol webst* olivine websterite; *harz* harzbugite; *protogr* protogranular; *porphyr* porphyroclastic; *interst* interstitial; + present; – absent; *ol* olivine; *opx* orthopyroxene; *cpx* clinopyroxene; *amph* amphibole; *phlog* phlogopite

Group	Group 1a		Group 1b		Group 1c			Group 2	
Sample	GBX-5	GBX-6	GBX-4	GBX-7	GBX-8	GBX-2	GBX-10	GBX-3	GBX-12
Rock type	Wehrlite	Wehrlite	Lherz	Lherz	Lherz	Lherz	Ol webst	Harz	Harz
Texture	Protogr	Porphyr	Porphyr	Porphyr	Protogr	Protogr	Protogr	Protogr	Protogr
Grain size (mm)	3–4	3–4	1–2	2–3	4–6	3–4	3–4	4–6	4–6
Special features	Large, anhedral amph	Euhedral phlog	Interst amph + phlog	Interst amph + phlog	–	Anhedral amph	Reacted spinel; amph + apatite	–	–
Glass, carbonate	+, –	+, +	–, +	–, –	–, –	+, –	+, +	–, –	–, –
Fo# (ol)	90.0	89.5	89.0	90.8	90.9	90.1	91.1	91.7	92.1
Mg# (sp)	–	–	72	72	78	79	76	70	64
Cr# (sp)	53	–	22	35	16	9	24	35	56
Equilibration temperatures (°C)									
From Wells (1977)	979	973	1005	1015	972	973	973	871	861
Calculated modes %; by least squares mixing using mineral and whole-rock analyses									
Ol	75.0	69.2	55.6	70.9	66.0	52.7	33.0	74.6	73.5
Opx	Trace	3.0	21.1	19.2	24.8	32.2	36.0	19.8	24.3
Cpx	15.9	25.4	20.3	6.2	7.5	7.4	25.6	4.2	1.6
Spinel	1.0	–	0.4	0.3	1.7	2.1	2.4	1.4	0.6
Amph	8.1	–	1.4	2.5	–	5.6	2.7	–	–
Phlog	–	2.4	1.0	0.7	–	–	–	–	–
Apatite	–	–	0.2	0.2	–	–	0.3	–	–
r^2	0.23	0.33	0.07	0.01	0.05	0.10	0.20	0.26	0.07

Lote 17 xenolith groups

Lote 17 spinel peridotite xenoliths are divided into two basic groups. Group 1 consists of fertile, hydrous peridotites, and Group 2 are infertile, anhydrous harzburgites (Table 1). Textures of Group 1 xenoliths are consistent with a complex metasomatic history involving variable extents of reaction of refractory lherzolite or harzburgite with carbonatitic melts. The reaction involves orthopyroxene + spinel + carbonatite melt that reacts to form Cr-, Na-rich diopside + olivine + pargasite/phlogopite + CO_2 (Green and Wallace 1988). Group 1 xenoliths are similar to amphibole–phlogopite–apatite lherzolite and wehrlite xenoliths from southeast Australia (Yaxley et al. 1991) and the Sahara Basin (Dautria et al. 1992), whose textures and mineralogy are attributed to carbonatite metasomatism. Group 1 xenoliths are further divided into three subgroups (a, b, c) based on distinctive textures and trace element chemistry (Table 1).

Group 1a xenoliths consist of protogranular to porphyroclastic, olivine-rich wehrlites that have a medium to coarse grain size (2–4 mm) and disseminated phlogopite (GBX-6) or amphibole (GBX-5). Sample GBX-6 has a weak planar fabric defined by tabular olivine and aggregates of phlogopite. Silicate glass is present mostly as small (~1 mm) melt pockets and veinlets. Carbonate fills vesicles in the glass. Group 1a xenoliths have a texturally well-equilibrated assemblage of olivine + Na-rich clinopyroxene + amphibole/phlogopite with minor amounts of orthopyroxene and spinel that indicate an advanced stage of carbonatite–peridotite reactions as suggested for southeast Australian (Yaxley et al. 1991) and Tanzanian (e.g., Rudnick et al. 1993) peridotite xenoliths.

Group 1b xenoliths consist of porphyroclastic lherzolites (GBX-4 and GBX-7) that have a medium grain size (~1–3 mm), and have interstitial amphibole and phlogopite. Accessory apatite is inferred to be present based on least squares analysis of mineral and whole-rock data (Table 1), but has not been identified in thin section. These samples also lack glass. Group 1b textures and mineralogy are consistent with an intermediate stage of carbonatite metasomatism, although interstitial amphibole + phlogopite may reflect previous metasomatism involving basaltic melts (e.g., Menzies et al. 1987) or H_2O-rich fluids (e.g., O'Reilly and Griffin 1988).

Group 1c xenoliths consist of a lherzolite (GBX-2) and an olivine websterite (GBX-10) that have coarse-grained (4–6 mm), protogranular textures. Anhydrous lherzolite GBX-8 is included in this group because of similar trace element chemistry. GBX-10 contains small (~0.5 mm), inclusion-rich, euhedral apatite. Group 1c xenoliths are interpreted to record an incipient stage of carbonatite metasomatism, based primarily on the presence of apatite and reacted Cr-spinels rimmed by relict amphibole and a fine-grained aggregate of silicate

glass, olivine, and clinopyroxene. Similar features have been observed in other carbonatite metasomatized xenoliths (e.g., Ionov et al. 1994; Chazot et al. 1996; Wiechert et al. 1997; Yaxley et al. 1997).

Group 2 consists of anhydrous harzburgites (GBX-3 and GBX-12) with coarse-grained (~4–6 mm), protogranular textures. Group 2 xenoliths are cpx-poor and lack hydrous phases, silicate glass, or carbonate. They are classed as cryptic metasomatized xenoliths (Dawson 1984) because they have anomalous enrichments in LILE and LREE.

Results

Mineral chemistry

Mineral and glass chemistry for Lote 17 xenoliths is presented in Tables 1–4. Olivine and orthopyroxene compositions range from Fo_{89} to Fo_{92} and Mg# = 88 to 91 (Tables 1 and 2). Olivine and orthopyroxene are more magnesian and spinel has higher Cr# in Group 2 harzburgites compared to Group 1 xenoliths, consistent with the former being residues from higher percentages of melt extraction. Amphiboles are pargasitic with 0.8–1.6% K_2O, 1.3–4.3% TiO_2, and 0.9–2.0% Cr_2O_3 (Table 3) and phlogopites are Cr-rich with 1.5–1.7% Cr_2O_3 and 2.6–3.5% TiO_2 (Table 3).

Clinopyroxene in Lote 17 xenoliths are Cr-diopsides with 0.65–2.1% Cr_2O_3, 0.6–2.9% Na_2O, and 1.9–6.7% Al_2O_3 (Table 2). Group 2 harzburgites have clinopyroxene with the lowest Na_2O (<1%) and Al_2O_3 (<2.5%) and highest CaO (>22%) contents. Spongy clinopyroxene rims have lower Na_2O and Al_2O_3, higher CaO and Cr_2O_3, and slightly higher MgO and TiO_2 than corresponding core compositions (Table 2). These characteristics are similar to clinopyroxene in peridotite xenoliths from Mongolia (Ionov et al. 1994; Wiechert et al. 1997) and the Sahara Basin (Dautria et al. 1992), and are thought to be caused by initial stages of carbonatite metasomatism-induced partial melting. Lote 17 clinopyroxenes are compared in Fig. 2 with clinopyroxenes from adakitic metasomatized peridotite xenoliths from northern Kamchatka (Kepezhinskas et al. 1995, 1996) and carbonatite metasomatized peridotite xenoliths from northern Tanzania (Rudnick et al. 1993), southeast Australia (Yaxley et al. 1991), Sahara Basin (Dautria et al. 1992), and Mongolia (Ionov et al. 1994). The high SiO_2, Na_2O, and Cr_2O_3 (not shown) at a given Al_2O_3 content of Lote 17 Group 1 clinopyroxenes are most similar to those in carbonatite metasomatized xenoliths.

Glass compositions in Lote 17 Group 1 xenoliths are Na_2O-rich (4.7–7.7%), Al_2O_3-rich (20.5–22.8%) silicate melts with high CaO (4.3–10.4%) and TiO_2 (2.1–2.8%) and relatively low SiO_2 (50–53%; Table 4). They are strikingly similar to glass in carbonatite metasomatized peridotite xenoliths from Yemen (Chazot et al. 1996), southeast Australia (Frey and Green 1978; Yaxley et al. 1997; Eggins et al. 1998), and Mongolia (Ionov et al.

Table 2 Microprobe analyses of pyroxenes (wt%). *Opx*, *Cpx* core analyses; *Cpx rim* spongy rims. Mg# = [Mg/(Mg + Fe^{2+})] × 100. Fe^{2+} by charge balance (Lindsley 1983)

Type	Group 1a			Group 1b				Group 1c				Group 2			
Sample	GBX-5			GBX-6			GBX-4		GBX-7		GBX-2		GBX-8		GBX-10			GBX-3		GBX-12	
Phase	Opx	Cpx	Cpx rim	Opx	Cpx	Cpx rim	Opx	Cpx	Opx	Cpx	Opx	Cpx	Opx	Cpx	Opx	Cpx	Cpx rim	Opx	Cpx	Opx	Cpx
SiO_2	56.51	53.11	52.37	56.97	53.72	52.84	54.73	52.65	55.83	52.97	54.89	51.96	55.61	52.54	51.63	55.74	52.20	51.50	56.37	54.29	57.33	54.22
TiO_2	0.11	0.33	0.51	0.09	0.28	0.32	0.25	0.71	0.11	0.42	0.12	0.59	0.09	0.40	0.60	0.06	0.25	0.27	0.06	0.14	0.01	0.14
Al_2O_3	2.27	4.12	2.87	1.61	4.45	2.31	3.71	5.22	3.26	5.54	4.28	6.65	4.25	5.72	4.60	3.89	6.13	3.95	2.37	2.43	1.39	1.90
Cr_2O_3	0.51	1.68	1.84	0.38	1.82	2.13	0.36	1.34	0.62	1.55	0.28	0.65	0.45	0.96	1.23	0.55	1.34	1.54	0.31	0.74	0.42	1.09
FeO	6.36	3.66	3.42	6.34	3.52	3.22	7.04	3.74	5.52	2.98	5.95	2.77	5.57	2.69	2.85	5.68	2.75	2.78	5.57	1.90	5.37	1.70
MnO	0.18	0.15	0.12	0.19	0.13	0.12	0.16	0.11	0.13	0.11	0.15	0.11	0.12	0.07	0.06	0.14	0.08	0.09	0.14	0.06	0.09	0.08
MgO	34.01	15.63	16.28	33.70	15.27	16.72	32.29	15.20	33.71	15.22	32.57	14.88	33.29	15.55	16.90	34.12	15.27	16.62	34.92	16.93	34.84	17.18
CaO	0.74	18.92	21.19	0.73	17.89	21.34	0.74	18.43	0.83	17.97	0.69	19.41	0.72	19.89	20.89	0.68	19.36	22.02	0.40	23.25	0.39	22.81
Na_2O	0.17	2.30	1.06	0.21	2.86	1.18	0.13	2.15	0.17	2.31	0.11	1.80	0.09	1.82	0.55	0.14	2.16	0.63	0.03	0.61	0.07	0.93
Total	100.85	99.89	99.66	100.21	99.95	100.17	99.41	99.56	100.18	99.08	99.02	98.81	100.20	99.63	99.29	101.00	99.55	99.39	100.17	100.35	99.92	100.05
Mg#	90.5	88.4	89.4	90.4	88.5	90.3	89.1	87.9	91.6	90.1	90.7	90.5	91.4	91.2	91.4	91.5	90.8	91.4	91.8	94.1	92.0	94.8

Table 3 Microprobe analyses (wt%) of amphiboles and phlogopites

Sample	GBX-5	GBX-4	GBX-7	GBX-2	GBX-10	GBX-6	GBX-7
	Amphibole					Phlogopite	
SiO_2	44.95	42.66	43.66	43.23	44.03	40.03	38.84
TiO_2	1.77	4.27	2.30	2.36	1.31	2.61	3.53
Al_2O_3	12.85	14.20	14.09	15.89	15.21	16.20	16.82
Cr_2O_3	2.08	1.36	1.96	0.90	1.83	1.48	1.71
FeO	4.61	4.74	3.88	4.11	3.94	4.59	4.01
MnO	0.11	0.05	0.08	0.08	0.09	0.04	0.00
MgO	17.92	16.11	17.53	17.19	18.13	22.10	21.21
CaO	9.88	10.10	10.18	10.61	10.29	0.04	0.04
Na_2O	3.63	3.23	3.43	3.52	3.86	0.79	0.72
K_2O	1.45	1.61	1.56	0.81	0.72	8.62	8.65
Total	99.24	98.34	98.67	98.70	99.39	96.50	95.54

1994). In contrast, Lote 17 xenolith glasses are very different from glass in adakite metasomatized xenoliths from northern Kamchatka (Kepezhinskas et al. 1995) indicating a metasomatic component other than a slab-derived melt. Lote 17 xenolith glass is also distinct from the host basanite, ruling out any direct origin by host lava infiltration (compare host lava in Table 5). Glass compositions in Lote 17 amphibole-bearing xenoliths are CaO- and Na_2O-rich, whereas glass in the phlogopite-bearing xenoliths are distinctly K_2O-rich. This supports the interpretation that the glass formed by the breakdown of amphibole + phlogopite (± clinopyroxene) just prior to or during ascent in the host magma (e.g., Francis 1976; Chazot et al. 1996; Yaxley et al. 1997) or by metasomatism-induced partial melting (e.g., Ionov et al. 1994).

Equilibration temperatures were calculated using two-pyroxene thermometry (Wells 1977) and are given in Table 1. Group 2 anhydrous harzburgites yield the lowest temperatures at 860 to 870 °C, whereas Group 1 peridotites yield higher temperatures of 970 to 1015 °C (Table 1). Equilibration pressures cannot be reliably calculated because Lote 17 peridotite xenoliths lack garnet; however, spinel peridotites with Cr# < 35 are only stable in the pressure range of 0.8 to 2.5 GPa (Webb and Wood 1986). Lote 17 spinel peridotites are

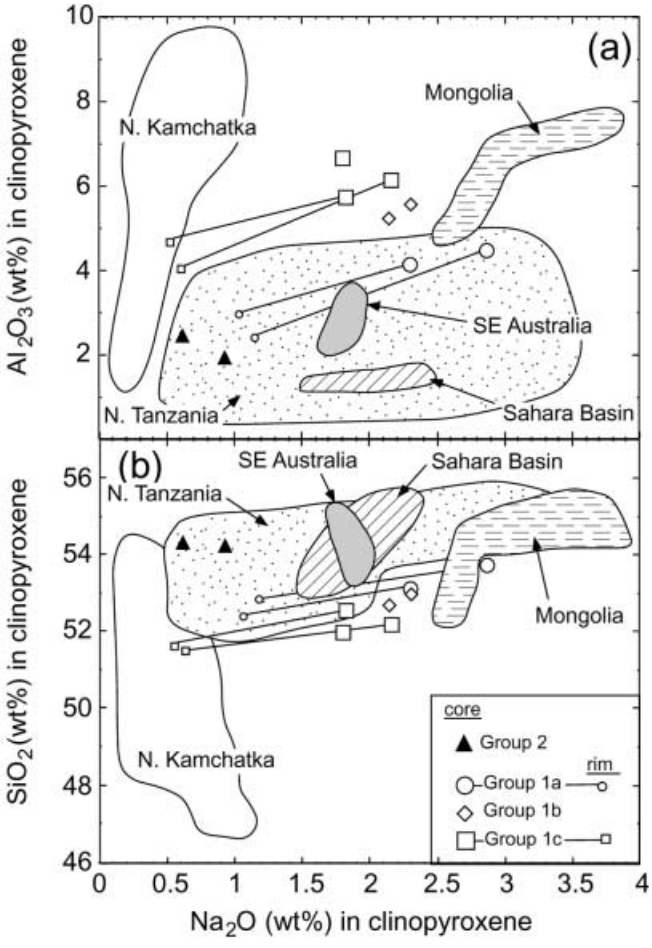

Fig. 2a,b Plots of Al_2O_3 **a** and SiO_2 **b** vs. Na_2O (wt%) in clinopyroxene from Lote 17 peridotite xenoliths. Symbols are given in the SiO_2 vs MgO plot (*open circles* Group 1a; *open diamonds* Group 1b; *open squares* Group 1c; *filled triangles* Group 2). Lines connect rim (*small symbols*) and core analyses (*large symbols*). Fields for clinopyroxene from adakite metasomatized xenoliths from northern Kamchatka (*open*; Kepezhinzkas et al. 1995, 1996) and carbonatite metasomatized xenoliths from northern Tanzania (*stipple*; Rudnick et al. 1993), southeast Australia (*solid gray*; Yaxley et al. 1991), Sahara Basin (*diagonal lines*; Dautria et al. 1992), and Mongolia (*thick horizontal lines*; Ionov et al. 1994)

Table 4 Microprobe analyses of glass (wt%) from Lote 17 xenoliths compared to other peridotite xenolith localities. Glass analyses from hydrous spinel lherzolite xenoliths from southeast Australia (Yaxley et al. 1997) and Yemen (Chazot et al. 1996). Mean adakitic glass from adakite metasomatized peridotite xenoliths from northern Kamchatka (Kepezhinskas et al. 1995)

Sample	GBX-5	GBX-6	GBX-2	GBX-10	SE Australia glass (71004)	SE Australia glass (70997)	Yemen mean glass	N Kamchatka adakite glass
	Amph	Phlog	Amph	Amph	Amph + phlog	Amph	Amph	
SiO_2	51.18	52.90	51.22	49.89	51.32	52.25	52.44	64.76
TiO_2	2.58	2.11	2.84	1.71	2.73	2.30	1.39	0.60
Al_2O_3	20.76	20.71	20.56	22.75	20.99	21.05	20.27	18.52
FeO	3.52	2.98	3.79	3.17	3.08	5.16	3.41	2.41
MnO	0.08	0.09	0.07	0.08	–	–	0.12	0.05
MgO	3.41	2.56	4.28	3.61	2.81	2.86	3.00	0.70
CaO	7.11	4.26	10.38	8.49	4.18	5.96	7.01	2.13
Na_2O	7.60	7.74	4.70	7.11	6.82	5.77	6.95	6.88
K_2O	3.08	6.07	1.16	1.87	5.81	3.61	1.54	1.54
P_2O_5	0.19	0.02	0.04	0.32	0.54	1.16	0.63	–
Total	99.50	99.43	99.04	99.00	98.27	100.12	96.76	97.59

Table 5 Major (wt%) and trace element (ppm) concentrations for Lote 17 peridotite xenoliths. Major elements normalized to 100%. Trace elements by INAA are Sc, Cr, Ni, Co, Ba, Cs, Ta, Hf, La, Sm, Eu, Yb, and those with *. Trace elements by ICP-MS are Y, Rb, Sr, Nb, Zr, Ce, Pr, Nd, Gd, Tb, Dy, Ho, Er, Lu, U, Th, Pb, and those with †. – below detection limits; *blank spaces* element not determined

Type	Group 1a		Group 1b		Group 1c			Group 2		Host lava
Sample	GBX-5	GBX-6	GBX-4	GBX-7	GBX-8	GBX-2	GBX-10	GBX-3	GBX-12	GB-1
SiO_2	42.28	42.97	45.27	44.17	44.18	45.37	47.85	43.49	44.56	44.92
TiO_2	0.23	0.11	0.36	0.09	0.07	0.15	0.10	0.03	0.04	2.98
Al_2O_3	1.83	1.50	2.20	1.55	2.36	3.96	3.80	0.99	0.64	13.91
FeO	8.78	8.93	9.30	7.76	7.83	7.93	6.50	7.98	6.94	10.08
MnO	0.19	0.08	0.04	0.13	0.20	0.18	0.00	0.17	0.14	0.17
MgO	40.64	39.79	37.21	43.56	42.74	39.02	34.33	45.39	46.48	7.56
CaO	4.26	4.68	4.20	1.70	1.68	2.27	5.16	1.06	0.44	12.41
Na_2O	0.72	0.86	0.45	0.26	0.20	0.42	0.64	0.10	0.07	3.33
K_2O	0.15	0.18	0.16	0.10	0.06	0.12	0.09	0.02	0.02	2.59
P_2O_5	–	–	0.08	0.06	–	–	0.12	–	–	1.19
Sc	17.7	12.7	7.5	9.7	10.6	17.3	18.4	8.2	7.3	11.8
Cr	3846	4423	2680	2424	2734	2187	7570	3139	2823	229
Ni	2069	2072	2177	2070	2330	2228	1772	2582	2350	214
Co	112	109	115	109	116	112	99	129	113	42
Y	4.23	4.18	2.90	2.00	1.17	4.22	3.68	0.22	0.12	
Ba	9.4	54.6	15.6	16.4	7.2†	2.2†	6.6	3.4†	3.2	754
Cs	0.004	0.088	0.013	0.011	0.030	0.014	0.016	0.002†	0.011	0.91
Rb	0.27	3.14	1.15	0.90	0.13	0.06	0.26	0.11	0.10	
Sr	86.3	97.7	50.1	32.0	15.2	33.0	146	2.4	3.7	1279
Nb	12.2	9.2	1.4	1.4	0.41	0.98	0.72	0.35	0.21	
Ta	1.31	0.95	0.108	0.047	0.010	0.045	0.009†	0.023	0.012	4.6
Zr	105	91	15	5.5	4.0	8.0	8.7	2.1	1.8	
Hf	1.50	1.59	0.487	0.128	0.108	0.243	0.217	0.037	0.044	8.1
La	2.59	2.99	1.30	0.77	1.50	2.06	10.4	0.134†	0.202†	53.4
Ce	7.51*	8.94	4.09*	2.53	2.17	4.86	22.1	0.28	0.38	111
Pr			0.680	0.430	0.163	0.541	2.21	0.032	0.051	
Nd	5.65*	6.78*	3.50*	2.32	0.617	1.99*	7.36	0.128	0.193	51.2
Sm	1.62	2.05	1.09	0.637	0.144	0.550	0.859	0.031†	0.045†	10.5
Eu	0.539	0.679	0.404	0.200	0.053†	0.191	0.233†	0.011†	0.018†	3.40
Gd			1.00	0.523	0.198	0.656	0.574	0.038		
Tb	0.189	0.252	0.155*	0.079	0.035	0.119*	0.099	–	–	1.20
Dy	0.829	1.083	0.770	0.379	0.238	0.788	0.508	0.046		
Ho	0.129	0.163	0.131	0.062	0.050	0.171	0.104	0.010		
Er	0.272	0.319	0.288	0.154	0.148	0.495	0.281	0.026		
Yb	0.205	0.213	0.165	0.144	0.181	0.488	0.273†		0.031	1.46
Lu	0.028	0.027	0.022*	0.023	0.031	0.073*	0.043	–	–	0.178
U	0.051	0.111	0.069	0.043	0.061	0.102	0.396	–	0.006*	2.01
Th	0.137	0.114	0.036	0.032	0.310	0.370*	1.94	0.071	0.050	7.39
Pb	0.125	0.119	0.047	0.035	0.172	0.096	0.148	0.105	0.041	
Ca/Al	3.14	4.21	2.58	1.48	0.96	0.77	1.84	1.45	0.94	
Na/Al	0.55	0.80	0.29	0.23	0.12	0.15	0.24	0.14	0.16	
Nb/Ta	9.3	9.7	12.6	29.9	41.2	21.8	79.9	15.0	17.1	
Sm/Hf	1.08	1.29	2.23	4.98	1.34	2.26	3.96	0.83	1.02	
Zr/Hf	69.7	57.5	31.3	43.2	37.1	32.9	40.2	55.5	40.9	
Ti/Eu	2539	1007	5360	2638	8031	4802	2575	18530	11657	

assumed to have equilibrated at pressures ranging from 1 to 2 GPa. This is consistent with minimum pressures of ~1.9 GPa for Pali–Aike garnet peridotite xenoliths (Stern et al. 1999).

Major element chemistry

Whole-rock major element analyses of Lote 17 peridotite xenoliths are given in Table 5. Lote 17 xenoliths form negative correlations on plots of Al_2O_3, CaO, Na_2O, and TiO_2 versus MgO (Fig. 3) that are similar to those for spinel peridotites on a global basis (Maaløe and Aoki 1977; McDonough 1990). The negative trends in Fig. 3 indicate variable extents of melt depletion of fertile mantle (McDonough 1990). Group 1 Lote 17 xenoliths are more fertile with respect to basaltic components (e.g., high Al_2O_3, CaO, Na_2O, TiO_2, and K_2O) than Group 2 xenoliths, consistent with their higher modal abundance of clinopyroxene and minor abundances of amphibole ± phlogopite ± apatite. Carbonatite metasomatism is recognized by anomalously high Ca/Al (3.1–4.2) and Na/Al (0.55–0.80) in Group 1a xenoliths compared to the global average (1.28 and 0.15, respectively; McDonough 1990) and are similar in major element composition to carbonatite metasomatized

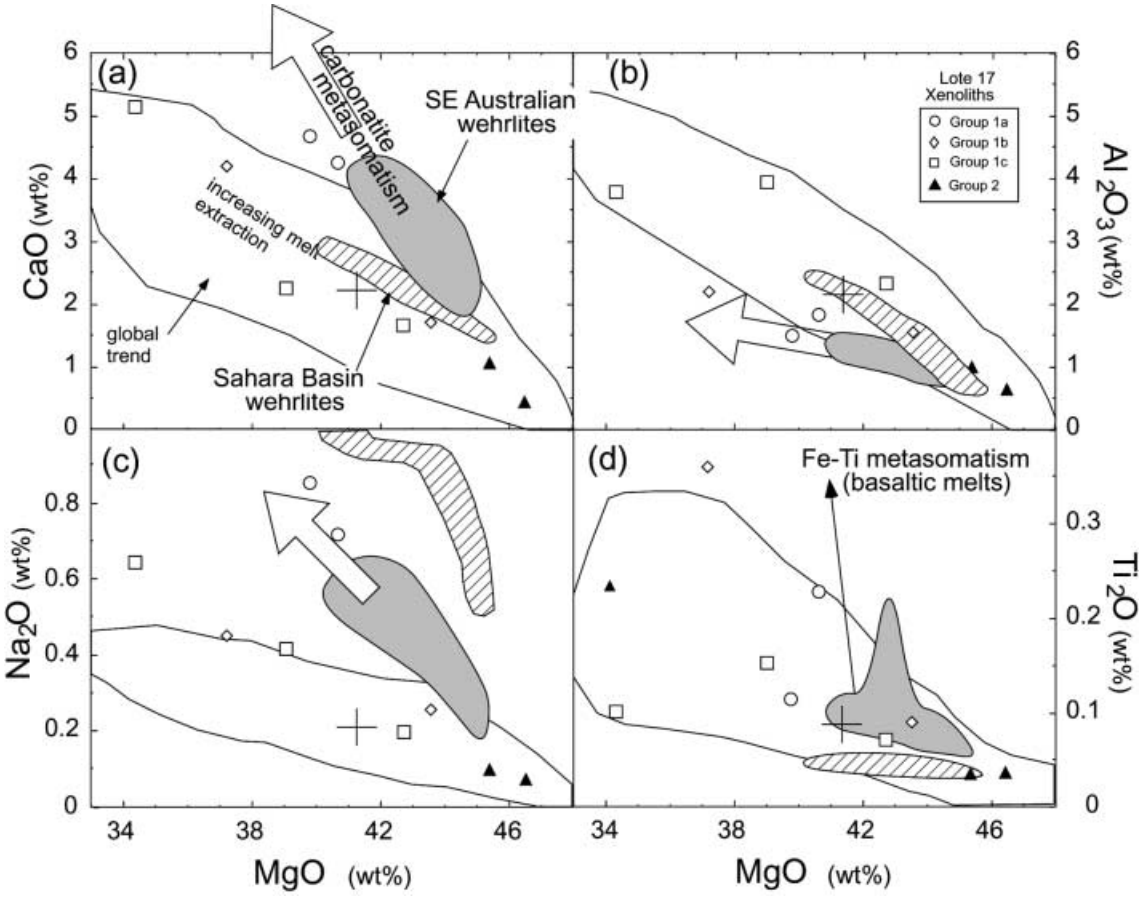

Fig. 3a–d Variation diagram for whole-rock CaO **a**, Al_2O_3 **b**, Na_2O **c**, and TiO_2 **d** (wt%) plotted against MgO (wt%) for Lote 17 peridotite xenoliths. Fields and symbols as in Fig. 2. *Open white area* shows global trend from Maaløe and Aoki (1977) and McDonough (1990). *Large cross* is the global median spinel peridotite xenolith composition of McDonough (1990). *Large, open arrows* indicate trends predicted for carbonatite metasomatism (in **a**, **b**, and **c**) (e.g., Yaxley et al. 1991). *Thin, black arrows* in **d** indicate trend for Fe–Ti basaltic melt metasomatism (e.g., Menzies et al. 1987)

xenoliths from southeast Australia (Yaxley et al. 1991). Overall, Groups 1b and 1c xenoliths are similar to global average spinel peridotite compositions in terms of major elements. One exception is sample GBX-4 from Group 1b. This sample has moderately high Ca/Al (2.58) and Na/Al (0.29), but also has high whole-rock FeO (9.3%) and TiO_2 (0.36%) concentrations (Fig. 3 and Table 5) and has amphibole with the highest TiO_2 concentration (4.27%, Table 3). These characteristics are consistent with an earlier basaltic melt metasomatism (e.g., Menzies et al. 1987) that was overprinted by more recent carbonatite metasomatism.

Trace element chemistry

Trace element analyses are given in Tables 5 and 6 and illustrated in Figs. 4 and 5. All Lote 17 peridotite xenoliths are LILE- and LREE-enriched, but Group 1 xenoliths have significantly higher incompatible trace element concentrations than Group 2 xenoliths.

Group 1a xenoliths are distinguished by slight LREE-depleted ($(La/Sm)_n = 0.9–1$) and very steep MREE to HREE [$(Gd/Yb)_n = 6–8$] patterns (Fig. 4a). HREE are ~0.8× chondrite. They have large positive Nb, Ta, Zr, and Hf, and negative Th and Ti anomalies relative to LILE and LREE (Fig. 5a) that lead to low Sm/Hf (~1.2) and Ti/Eu (1000–2500) ratios. HFSE are also fractionated from each other as Nb/Ta (~9.5) and Zr/Hf (57–70) ratios are significantly lower and higher, respectively, than chondritic ratios (Nb/Ta = 17.6; Zr/Hf = 36; McDonough 1990). High concentrations of HFSE reflects the high modal abundance of clinopyroxene, amphibole, and phlogopite. High Ba and Rb in GBX-6 reflects modal phlogopite. Trace element analyses of clinopyroxene and phlogopite separates from GBX-6 show that clinopyroxene can account for most of the REE, Sr, Ti, and Hf concentration in the whole rock (Table 6 and Fig. 6a). Mass balance deficiencies in Ba, Rb, Nb, and Ta are probably an artifact of small errors in the least squares calculation for modal phlogopite or possibly due to presence of undetectably thin reaction coatings of Ti-oxides and phlogopite on spinel or an enriched grain boundary component (e.g., Bodinier et al. 1996; Bedini and Bodinier 1999). Significant mass balance deficiencies in Th and U could be explained by undetected accessory apatite or an enriched grain

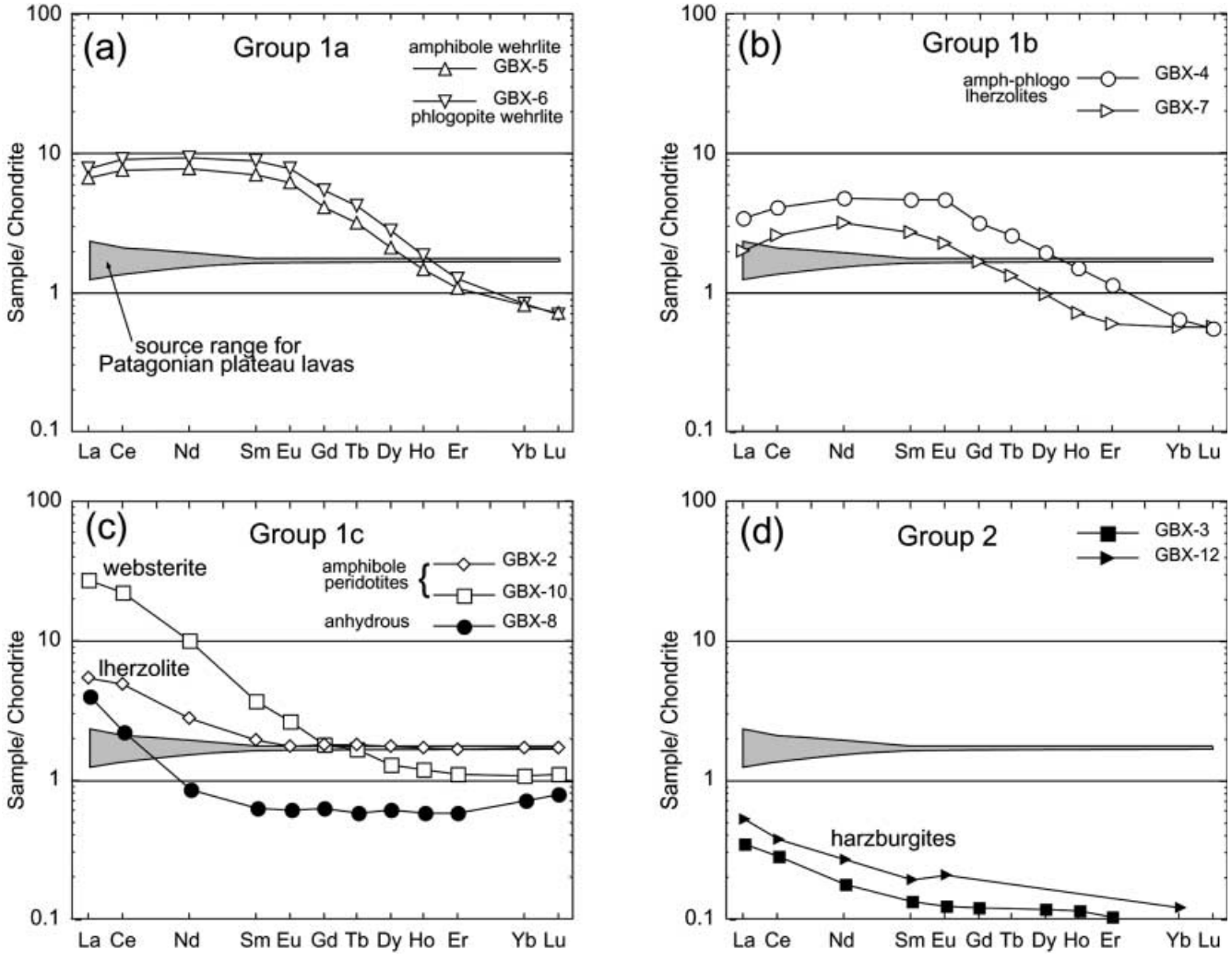

Fig. 4a–d Leedy chondrite normalized REE patterns for whole-rock Lote 17 peridotite xenoliths: **a** Group 1a wehrlites, **b** Group 1b amphibole–phlogopite lherzolites, **c** Group 1c amphibole peridotites, and **d** Group 2 anhydrous harzburgites. Also shown is the range of mantle compositions (*light gray pattern*) suitable for the Neogene Patagonian plateau lavas, based on trace element modeling of Gorring and Kay (2000). Normalization factors are from Masuda et al. (1973) and are La (0.378), Ce (0.978), Nd (0.716), Sm (0.23), Eu (0.0866), Gd (0.311), Tb (0.0589), Dy (0.385), Ho (0.0858), Er (0.251), Yb (0.249), Lu (0.0387). Factor for Ho was extrapolated

boundary component (e.g., O'Reilly et al. 1991; Bedini and Bodinier 1999).

Group 1b xenoliths have concave downward LREE [$(La/Sm)_n \sim 0.75$] and moderately steep HREE [$(Gd/Yb)_n = 2.5–4$] patterns (Fig. 4b). HREE are $\sim 0.5\times$ chondrite. They also have negative Th and small positive P anomalies (Fig. 5c). GBX-4 has near chondritic ratios for Zr/Hf (31) and Nb/Ta (12.6), slightly subchondritic Ti/Eu (5360) ratios, and small depletions in Zr, Hf, and Ti relative to LILE and REE. In contrast, GBX-7 has large negative Zr, Hf, and Ti anomalies that lead to high Sm/Hf (5) and low Ti/Eu (2640) ratios. Modal phlogopite and amphibole in Group 1b xenoliths explains high concentrations of Rb, Ba, and K. Apatite was not identified, but 0.2% modal apatite is calculated to account for $\sim 0.07\%$ P_2O_5 (see Table 1).

Group 1c xenoliths are easily recognized by their pronounced concave upward LREE pattern with steep LREE [$(La/Sm)_n = 3–6$] and flat MREE to HREE [$(Gd/Yb)_n = 1–1.5$] (Fig. 4c). HREE are 0.7–2× chondrites. They also have large negative Rb, Ba, Nb, Ta, Zr, and Hf anomalies and positive Th and U anomalies (Fig. 5e) that result in high Sm/Hf (2–4) and Nb/Ta (21–80), and low Nb/La (0.07–0.5). Near-chondritic ratios for Zr/Hf ($\sim$38) and variably negative Ti anomalies lead to Ti/Eu ratios from $\sim$2600 to $\sim$4800. Figure 6b shows that clinopyroxene separates from GBX-10 can account for 100% of the REE, Sr, and Hf, and $\sim$75% of Th, U, Ta, Zr, and Ti in the whole rock. The high Th, U, and LREE contents of the cpx separates is likely due to micro-inclusions of apatite that were not identified when hand-picked. The small amount of amphibole ($\sim$3%) and apatite ($\sim$0.3) in GBX-10 can account for mass balance deficiencies in Rb, Ba, K, Nb, Ta, Zr, and Ti (e.g., O'Reilly et al. 1991; Rudnick et al. 1993; Ionov and Hofmann 1995).

Group 2 harzburgite xenoliths (GBX-3 and GBX-12) have LREE-enriched patterns [$(La/Yb)_n = 3–5$] at very

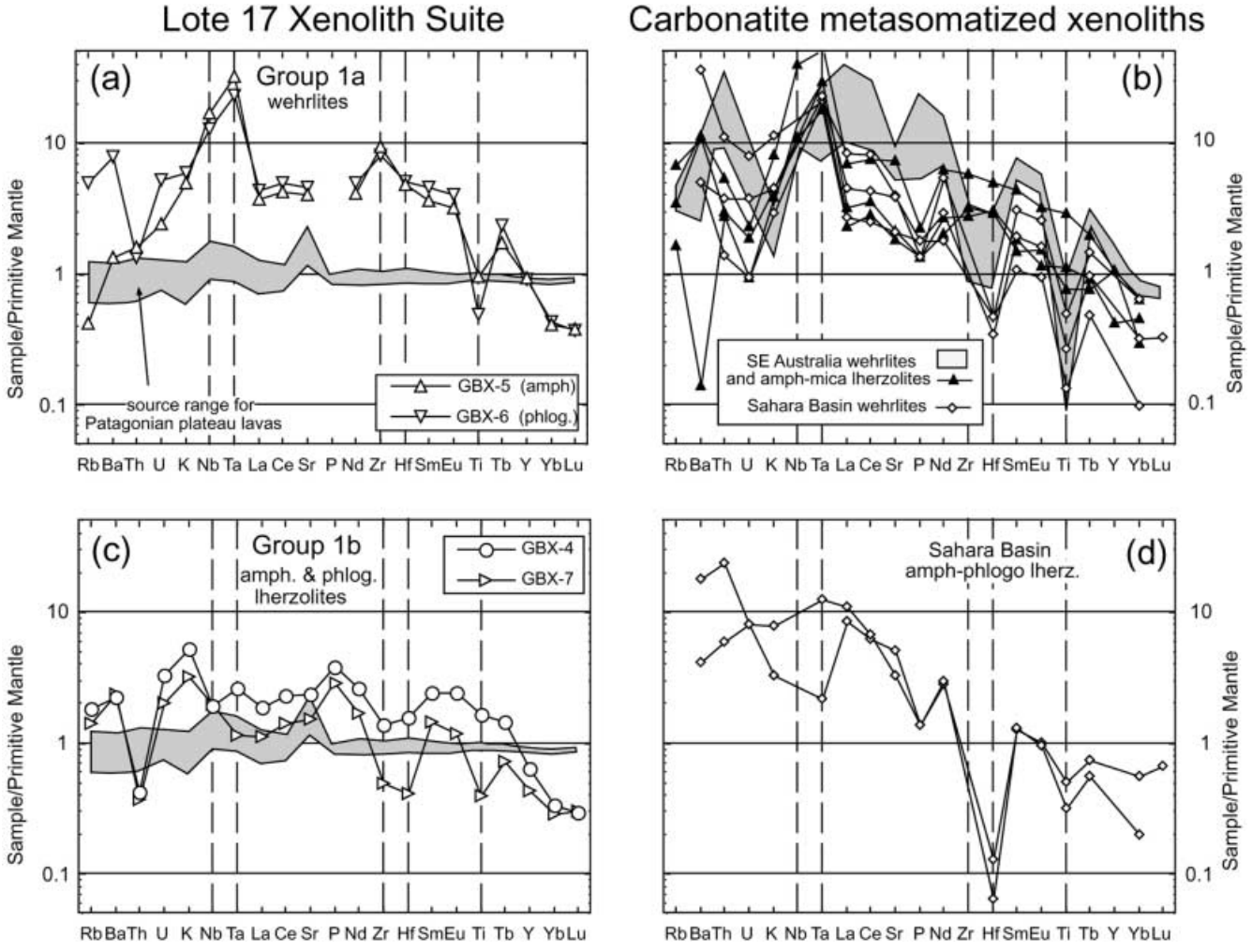

Fig. 5a–d Primitive mantle normalized trace element patterns for whole-rock Lote 17 peridotite xenoliths (**a**, **c**, **e**, **g**) compared to other carbonatite metasomatized xenoliths (**b**, **d**, **f**) from southeast Australia (O'Reilly and Griffin 1988; Yaxley et al. 1991), Sahara Basin (Dautria et al. 1992), and northern Tanzania (Rudnick et al. 1993). Also plotted for comparison **h** are arc fluid/melt metasomatized spinel peridotites from the Luzon arc (Maury et al. 1992). Symbols for Lote 17 xenoliths as in Fig. 4. Also shown is the range of mantle compositions (*light gray*) suitable for the Neogene Patagonian plateau lavas (Gorring and Kay 2000). All abundances normalized to the primitive mantle composition of Sun and McDonough (1989). *Dashed vertical lines* are for highlighting HFSE behavior

low concentrations of 0.1–1× chondrite (Figs. 4d and 5g). Ba, Th, and Ta are enriched relative to LREE, and HREE are very depleted at 0.1–0.2× chondrite.

Sr–Nd isotopes

Sr and Nd isotope data for Lote 17 xenoliths and the host basanite are presented in Table 7 and plotted in Fig. 7. Lote 17 xenoliths have $^{87}Sr/^{86}Sr$ ratios that range from 0.70294 to 0.70342 and ε_{Nd} values from +3.0 to +6.6 for whole-rock and mineral separates. Isotopic data for Pali–Aike peridotite xenoliths and Neogene Patagonian plateau lavas are shown as fields on Fig. 7 for comparison. Group 1a xenolith GBX-6 has the lowest whole-rock $^{87}Sr/^{86}Sr$ ratio (0.70294) and a relatively high ε_{Nd} (+6.2) value. Clinopyroxene separates from GBX-6 also have low $^{87}Sr/^{86}Sr$ ratios (0.70297) and the highest ε_{Nd} (+6.3). Phlogopite separates from GBX-6 have a slightly higher $^{87}Sr/^{86}Sr$ ratio (0.70315) and considerably lower ε_{Nd} (+3.4). Except for sample GBX-2 ($^{87}Sr/^{86}Sr = 0.70304$), samples from Groups 1b, 1c, and GBX-17 all have significantly higher whole rock $^{87}Sr/^{86}Sr$ (~0.7034) and lower ε_{Nd} (~+3.1) ratios than Group 1a xenoliths.

The highly variable and enriched trace element signatures of Lote 17 xenoliths coupled with their isotopically "depleted" signatures suggests that metasomatism was a relatively recent event. The low $^{87}Sr/^{86}Sr$ ratio of GBX-6 phlogopite places some constraints on the timing of carbonatite metasomatism. An $^{87}Rb/^{86}Sr$ ratio of 1.61, and assuming a MORB-like initial $^{87}Sr/^{86}Sr$ ratio of ~0.7026, yields a maximum model age of ~25 Ma for crystallization of the phlogopite in GBX-6. We suggest that carbonatite metasomatism beneath Lote 17 was associated with extensive Neogene plateau magmatism in this region. Similarly, the timing of lithospheric

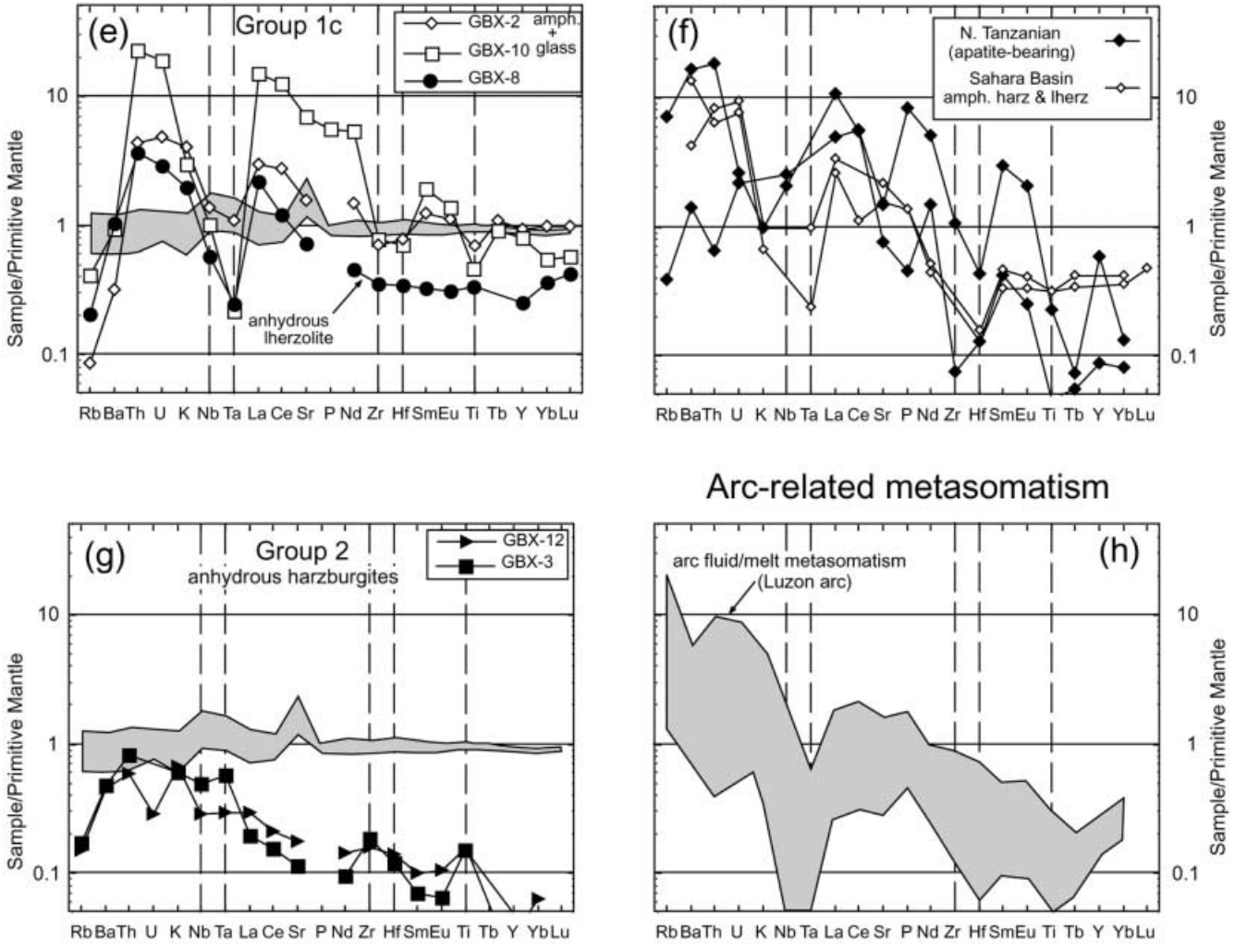

Fig. 5 (Contd.)

metasomatism in the Pali–Aike region is thought to associated with young (~1 Ma) plateau magmatism (Stern et al. 1999). However, unlike the Pali–Aike locality, the metasomatic fluids that affected the Lote 17 xenoliths were not cogenetic with the host lava (Fig. 7). As with most Patagonian post-plateau lavas, the host lava lacks chemical evidence for crustal contamination (Gorring and Kay 2000); thus the mantle source of the host lava was more isotopically "enriched" than that of the metasomatic component in the xenoliths.

Discussion and implications

Styles of lithospheric metasomatism

All Lote 17 peridotite xenoliths show evidence of metasomatic enrichment of an initially melt-depleted lithosphere. The overall pattern of metasomatic enrichment is a function of (1) modal mineralogy, (2) composition of the metasomatic fluids (e.g., carbonatitic, adakitic, and basaltic melts; H_2O- or CO_2-rich fluids), and (3) whether metasomatism occurs by closed-system addition (e.g., bulk mixing) or by open-system exchange (e.g., high melt/rock ratios; see Rudnick et al. 1993). The preservation of metasomatic reactions (e.g., reacted spinels, opx- and spinel-poor wehrlites with Na-rich cpx), high Ca/Al, Na/Al, La/Yb, Nb/La, Zr/Hf, and low Ti/Eu ratios, extreme fractionation of HFSE from LREE and LILE, and accessory amphibole, phlogopite, and apatite provide strong evidence for carbonatite-dominated metasomatism. In the next section, we discuss the four metasomatic styles displayed by the Lote 17 xenolith groups and give our preferred interpretations.

Group 1a wehrlites

The high Ca/Aland Zr/Hf and low Ti/Eu ratios like those in Lote 17 Group 1a wehrlites are commonly interpreted to result from carbonatite metasomatism (Yaxley et al. 1991; Dautria et al. 1992; Rudnick et al. 1993). Trace element patterns of Group 1a also show a striking similarity to carbonatite metasomatized

Table 6 Trace element (ppm) concentrations of mineral separates from Lote 17 xenoliths. Symbols as in Table 5

Sample Phase	GBX-10 Cpx	GBX-6 Cpx	Phlogo
Sc	67	43	2.7
Cr	9690	13843	11278
Ni	367	366	1554
Co	23	21	55
Y	9.67	12.2	0.40
Ba	2.7	1.3	1117
Cs	0.029	0.049	1.67
Rb	0.35	0.11	56.2
Sr	497*	396*	101
Nb	0.60	3.0	232
Ta	0.026	0.647	16.3
Zr	24	236	30
Hf	0.822	5.41	0.381
La	41.3	10.3	0.739†
Ce	82.6*	29.5*	0.631
Pr	8.6	5.3	0.158
Nd	27.0*	30.0*	0.653
Sm	3.24	7.66	0.121†
Eu	0.793	2.24	0.166†
Gd	2.15	6.62	0.104
Tb	0.285	1.00*	0.013
Dy	1.58	4.36	0.074
Ho	0.367	0.644	0.012
Er	1.06	1.20	0.031
Yb	1.05	0.637	0.030
Lu	0.147*	0.069*	0.005
U	1.17*	0.091	0.048*
Th	5.84*	0.319	0.018
Pb	0.472	0.418	0.559

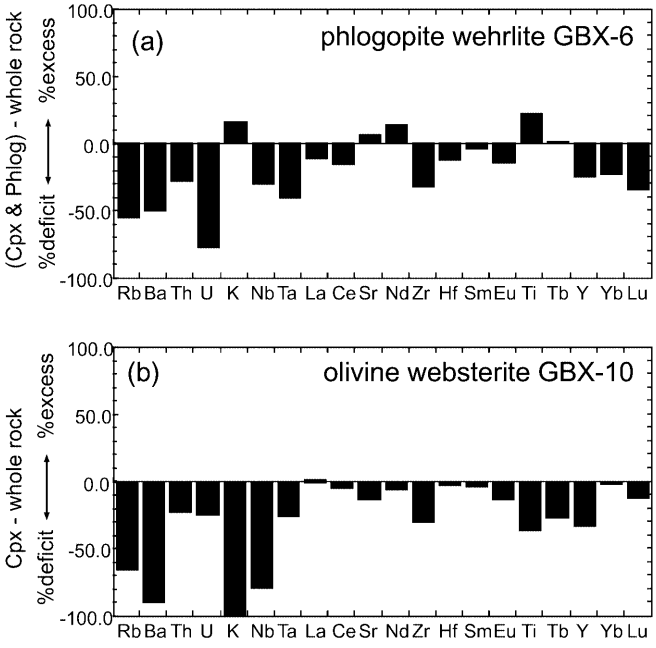

Fig. 6a,b Mass balance results for **a** Group 1a sample GBX-6, and **b** Group 1c sample GBX-10 showing the net deficit or excess (%). Mass balance is calculated from modal abundance in Table 1 and trace element data for whole-rocks and mineral separates given in Tables 5 and 6. All other phases are assumed to have zero concentration. Significant net deficits for Rb, Ba, Nb, Ta, U, Th, and Zr in GBX-6 reflects two factors (1) small errors in the least square analysis for phlogopite; (2) modal glass ± apatite (not identified). Large net deficits for Rb, Ba, K, Nb, Ta, and Ti in GBX-10 reflects modal amphibole + glass. The fairly good mass balance for Th, U, and REE in GBX-10 suggests that the cpx separates contained apatite inclusions

amphibole–phlogopite wehrlites and lherzolites from southeast Australia (O'Reilly and Griffin 1988; Yaxley et al. 1991) and the Sahara Basin (Dautria et al. 1992) (Fig. 5a, b). Similarities include LREE enrichment with slightly concave downward REE pattern, positive Nb–Ta anomalies, negative Ti anomalies, and high Zr/Hf ratios. Like the Lote 17 Group 1a wehrlites, southeast Australian amphibole–phlogopite-bearing lherzolites have low Nb/Ta ratios and lack negative Zr and Hf anomalies (Fig. 5a, b).

Group 1a wehrlites are interpreted as the result of clinopyroxene, amphibole, and/or phlogopite precipitation during open-system carbonatite metasomatism. The low Nb/Ta ratios are best explained by precipitation of phlogopite or amphibole from a carbonatite melt (e.g., Ionov and Hofmann 1995). This is supported by experimental work that suggests Ta has higher K_d^{amph} values than for Nb in equilibrium with carbonatitic liquids (Green et al. 1992; Sweeney et al. 1992). Evidence for open-system carbonatite metasomatism also includes higher Ti/Eu at a given Ca/Al than would be expected for bulk mixing of carbonatitic melt with a depleted harzburgite (Fig. 8; Rudnick et al. 1993). The anomalously high Ti/Eu reflects open-system partitioning of Ti between carbonatite melt and newly formed clinopyroxene and amphibole, as these phases have a higher K_d values for Ti than for Eu (Rudnick et al. 1993 and references therein). Open-system metasomatism may also explain the high Zr/Hf and positive Zr anomalies (Fig. 5a) in Group 1a wehrlites. Zr has higher K_d^{cpx} and K_d^{amph} values than K_d^{MREE} in equilibrium with carbonatite melt (Green et al. 1992; Sweeney et al. 1992), thus precipitation of clinopyroxene and amphibole could generate positive Zr anomalies. The high Zr/Hf ratios suggests that the metasomatizing carbonatite melt had even higher Zr/Hf because K_d^{cpx} and K_d^{amph} are likely to be higher for Hf than for Zr in equilibrium with carbonatite melt (Hamilton et al. 1989).

Group 1b lherzolites

Group 1b lherzolites have trace element characteristics that are transitional between Groups 1a and 1c. Strongly concave downward LREE patterns and high Rb, Ba, K, U, and P contents reflect modal amphibole + phlogopite ± apatite. Sample GBX-7 has low Ti/Eu and high Nb/Ta ratios, and sample GBX-4 has high Ca/Al ratios. These characteristics are consistent with carbonatite metasomatism (Yaxley et al. 1991; Rudnick et al. 1993). Group 1b lherzolites also have trace element patterns similar to amphibole–phlogopite lherzolite xenoliths from the Sahara Basin (Fig. 5d). However, unlike other carbonatite metasomatized xenoliths, GBX-7 has

Table 7 Sr–Nd isotopic compositions for Lote 17 xenoliths, minerals, and host lava. *wr* Whole-rock; *cpx* clinopyroxene separate; *phlog* phlogopite separate. Sr–Nd isotopes by thermal ionization mass spectrometry at Cornell. Isotope ratios corrected for mass fractionation assuming $^{86}Sr/^{88}Sr = 0.1194$ and $^{146}Nd/^{144}Nd = 0.7219$. Average measured value for NBS987 Sr standard was $^{87}Sr/^{86}Sr = 0.710237 \pm 23$ (2σ) from April 1996 to August 1997 based on 28 analyses. The LaJolla Nd standard was $^{143}Nd/^{144}Nd = 0.511864 \pm 14$ (2σ) based on 10 analyses and 0.511817 ± 12 (2σ). Ames Nd standard was $^{143}Nd/^{144}Nd = 0.512131 \pm 14$ (2σ) based on 10 analyses. ε_{Nd} values calculated assuming LaJolla $\varepsilon_{Nd} = -15.15$ (Wasserburg et al. 1981)

Type	Sample	Phase	Rb (ppm)	Sr (ppm)	$^{87}Rb/^{86}Sr$	$^{87}Sr/^{86}Sr$	Nd (ppm)	Sm (ppm)	$^{147}Sm/^{144}Nd$	$^{143}Nd/^{144}Nd$	ε_{Nd}
Group 1a	GBX-6	Wr	3.14	97.7	0.0930	0.70294	6.78	2.05	0.1834	0.512958	+6.2
		Cpx	0.105	396	0.0008	0.70297	22.1	6.2	0.1701	0.512981	+6.6
		Phlog	56.2	101	1.6103	0.70315	0.653	0.121	0.1124	0.512816	+3.4
Group 1b	GBX-4	Wr	1.15	50.1	0.0664	0.70342	3.5	1.09	0.1889	0.512805	+3.2
Group 1c	GBX-2	Wr	0.060	33.0	0.0053	0.70305					
	GBX-10	Wr	0.260	146	0.0052	0.70339	7.36	0.859	0.0708	0.512793	+3.0
		Cpx	0.347	497	0.0020	0.70338	20.5	2.36	0.0698	0.512805	+3.2
Host lava	GB-1	Wr		1279		0.70380	51.2	10.5	0.1244	0.512726	+1.7

chondritic Ca/Al and Zr/Hf ratios and sample GBX-4 has near chondritic Zr/Hf and Ti/Eu ratios. These trace element signatures and the relatively high-Ti amphibole and phlogopite in Group 1b xenoliths (Table 3) indicate an older, Fe–Ti-rich, basaltic melt metasomatic component (e.g., Menzies et al. 1987) that was partially overprinted by more recent carbonatite metasomatism.

Group 1c lherzolites and websterite

The trace element characteristics of Group 1c xenoliths are consistent with the bulk addition of a small amount of HFSE-depleted, carbonatite melt (< 0.2%; Fig. 8) and the precipitation of apatite in the case of sample GBX-10. We envision metasomatism of Group 1c xenoliths by a carbonatite melt that had previously precipitated phlogopite ± amphibole + clinopyroxene in association with Groups 1a and 1b. Thus, the fractionated carbonatite melt would be strongly depleted in all HFSE, Rb, and Ba and enriched in Th, U, and LREE, had high Nb/Ta ratios, and may have been saturated with respect to apatite. Group 1c xenoliths also have lower Zr/Hf and Ca/Al (both near chondritic), and much higher Ti/Eu ratios than in Group 1a xenoliths that indicate a much smaller carbonatitic component (Fig. 8). The extreme enrichment in Th, U, and LREE, and depletion in HFSE is characteristic of apatite-bearing lherzolite and wehrlite xenoliths from southeast Australia (O'Reilly and Griffin 1988; Yaxley et al. 1991)

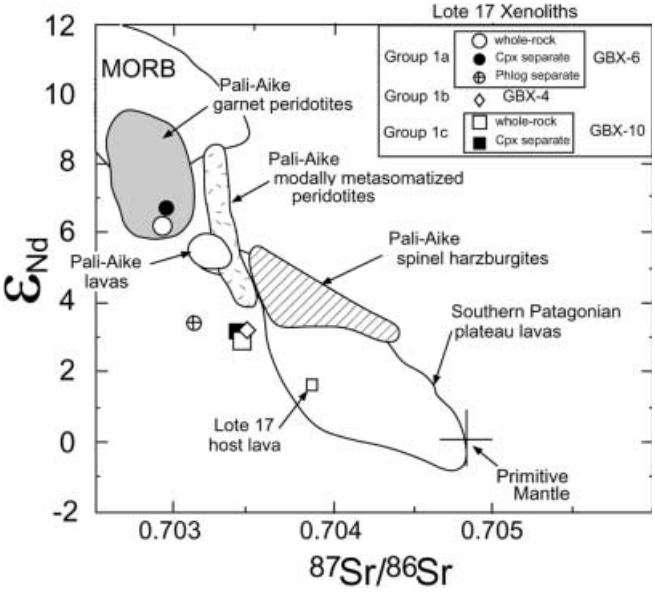

Fig. 7 Plot of ε_{Nd} versus $^{87}Sr/^{86}Sr$ for Estancia Lote 17 and Pali–Aike peridotite xenoliths (Stern et al. 1999) showing the relatively depleted isotopic signature of the southern Patagonian lithosphere compared to most Neogene Patagonian plateau lavas (Hawkesworth et al. 1979; Ramos and Kay 1992; Gorring and Kay 2000). Pali–Aike lava data from Stern et al. (1990). "Primitive mantle" composition (*large cross*) is from Zindler and Hart (1986). MORB data is compiled from the literature

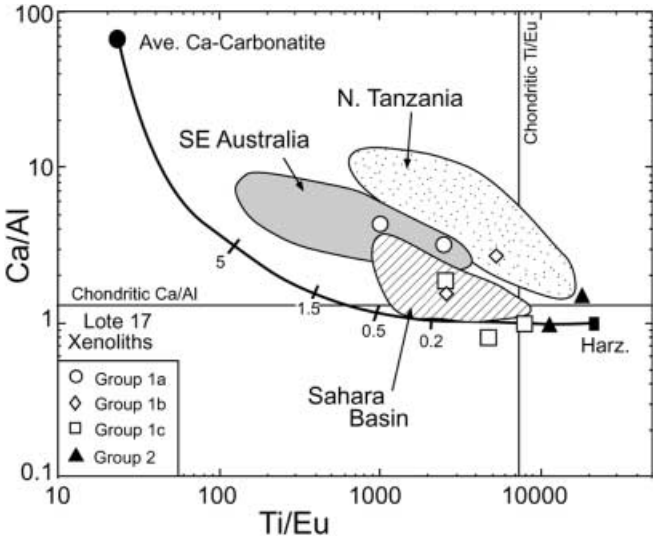

Fig. 8 Plot of Ca/Al versus Ti/Eu (after Rudnick et al. 1993) for Estancia Lote 17 peridotite xenoliths showing the overall similarity to other carbonatite metasomatized xenoliths from southeast Australia (*gray field*; Yaxley et al. 1991), northern Tanzania (*stippled field*; Rudnick et al. 1993), and the Sahara Basin (*diagonal ruled field*; Dautria et al. 1992). Bulk mixing curve is between average Ca-carbonatite (Wooley and Kempe 1989) and pyrolitic harzburgite (Harz.; after Rudnick et al. 1993). *Numbered ticks* on bulk mixing curve indicates percent of carbonatite in the mixture. Chondritic Ca/Al and Ti/Eu ratios from McDonough (1990)

and northern Tanzania (Rudnick et al. 1993), and amphibole harzburgites and lherzolites from the Sahara Basin (Dautria et al. 1992; Fig. 5e, f). Other possible interpretations include metasomatism by slab-derived, H_2O-rich fluids or arc-related silicate melts (e.g., basalts, adakites). These metasomatic agents would be LREE-enriched and HFSE-depleted, but would have difficulty explaining low LILE contents in Group 1c xenoliths. This is illustrated by comparing the pattern of metasomatized spinel lherzolites (both anhydrous and hydrous) from the Luzon arc (Maury et al. 1992) with Group 1c xenoliths (Fig. 5e, h).

Group 2 – anhydrous harzburgites

The anhydrous Group 2 harzburgite xenoliths (GBX-3 and GBX-12) have pronounced enrichments of LILE, HFSE, and LREE that are superimposed on an otherwise depleted chemistry and mineralogy. Thus, Group 2 harzburgites fit the definition of cryptic metasomatism (Dawson 1984). Cryptic metasomatism by H_2O- or CO_2-rich fluids enriched in LILE and LREE (e.g., Kempton 1987 and references therein), coupled with intrinsic positive HFSE anomalies in olivine and orthopyroxene (Rampone et al. 1991; McDonough et al. 1992; Sun and Kerrich 1995) could explain the data. Metasomatic reactions that affected the Group 1 xenoliths could have released CO_2-rich fluids (Green and Wallace 1988) to modify Group 2 harzburgites.

Model for metasomatism in the Patagonian lithosphere

We envision a model similar to those developed for the Saharan Basin (Dautria et al. 1992) and the West Eifel (Thibault et al. 1992) xenoliths, where thermal events caused partial melting of carbonated and/or hydrated components stored in the basal continental lithosphere. The model requires an initial melt-depleted, refractory harzburgitic or lherzolitic mantle beneath Patagonia (e.g., Stern et al. 1999) that has been recently metasomatized. The low $^{87}Sr/^{86}Sr$ ratios of Group 1a wehrlites indicate that the carbonatite metasomatic component was asthenosphere-derived and probably stored in the lithosphere during the early Neogene (~25 Ma). Asthenospheric upwelling associated with late Miocene main-plateau magmatism may have triggered partial melting of the stored carbonatite components and converted some of the mantle lithosphere into a heterogeneous assemblage of fertile, hydrous peridotites represented by Lote 17 Group 1 xenoliths. Most of the mantle lithosphere probably remains essentially as infertile, anhydrous peridotites with minor cryptic metasomatism similar to Group 2 xenoliths.

According to Wallace and Green (1988), small volumes of carbonatite melt are generated in equilibrium with amphibole lherzolite under $CO_2 \pm H_2O$-undersaturated conditions at depths between 60 and 90 km and temperatures of 950 to 1080 °C. Lithospheric thickness is thought to have been approximately ~70 km at this time, based on inferred melting depths of the Neogene plateau lavas (Gorring and Kay 2000). Therefore, LILE-, LREE-, Nb-enriched, and Ti-depleted carbonatite melts could easily have been generated and percolated upward through the lithosphere. Upon reaching ~60 km depth, reaction of carbonatite melt with refractory anhydrous harzburgite or lherzolite would produce amphibole- or phlogopite-bearing wehrlites and liberate CO_2-rich fluids (Wallace and Green 1988; Yaxley et al. 1991; Yaxley and Green 1996). In Patagonia, this process may have been continually fed by open-system addition of fresh carbonatite melts during extensive late Miocene main-plateau magmatism, thus producing the Group 1a amphibole and phlogopite wehrlites. Precipitation of phlogopite and amphibole to form Group 1a wehrlites, coupled with chromatographic effects during percolation through the lithosphere (e.g., Navon and Stolper 1987; Kelemen et al. 1990; Hauri and Hart 1994), would deplete the metasomatizing fluids in HFSE, Rb, and Ba. This would produce the systematic changes observed from Group 1a wehrlites to Group 1b amphibole–phlogopite lherzolites, and lead to the HFSE-depleted, LREE-, Th-, and U-enriched, Group 1c amphibole–apatite lherzolites. CO_2-rich fluids liberated from carbonatite–peridotite reactions may have caused cryptic metasomatism in the most infertile harzburgites and lherzolites.

Mantle metasomatism and Neogene plateau magma petrogenesis

The extreme chemical heterogeneity and the depleted Sr–Nd isotopic composition of Lote 17 xenoliths suggest that metasomatic components stored in the mantle lithosphere are neither the primary source nor an appropriate isotopically enriched contaminant for most Neogene Patagonian plateau lavas. This strongly contrasts with the close correspondence of regional isotopic and geochemical compositions of Cenozoic basalts and their entrained lithospheric mantle xenoliths from eastern Australia (e.g., O'Reilly and Zhang 1995) and eastern China (e.g., Tatsumoto et al. 1992). This difference is thought to reflect a larger contribution from OIB-like asthenospheric sources in the Patagonian slab window setting, the interaction with a younger, more "depleted" Patagonian continental lithosphere, and crustal contamination (Stern et al. 1990; Zartman et al. 1991; Gorring and Kay 2000).

Trace element evidence argues against carbonatite metasomatized lithosphere as the main source for Neogene Patagonian plateau lavas. First, primary mantle melts should have ratios of highly incompatible trace elements that reflect the mantle source composition provided that the bulk distribution coefficient is less than the melt fraction. Group 1 Lote 17 xenoliths have highly

variable incompatible trace element ratios that are outside the relatively narrow range displayed by Patagonian plateau lavas (Gorring and Kay 2000) and those of MORB and OIB (Sun and McDonough 1989). Second, Group 1 xenoliths are significantly more enriched in LILE and LREE and depleted in HREE compared to the inferred source of Patagonian plateau lavas based on trace element modeling (see Figs. 4 and 5; and Gorring and Kay 2000). However, the lithospheric mantle may represent a source for additional trace element-enriched components that could modify asthenospheric melts as they pass through the lithosphere.

Based on data presented here and on data for Pali–Aike peridotite xenoliths (Stern et al. 1989, 1999), there is little direct evidence for isotopically enriched components in the Patagonian backarc lithosphere from either slab-derived components or from ancient enrichment events (Fig. 8). Enriched and heterogeneous isotope ratios ($^{87}Sr/^{86}Sr = 0.7036–0.7047$; $\varepsilon_{Nd} = +5–0$) for most Late Miocene main-plateau lavas can be explained by crustal contamination of asthenosphere-derived melts (Gorring and Kay 2000). However, most of the younger, Pliocene post-plateau lavas have relatively homogeneous isotopic compositions ($^{87}Sr/^{86}Sr = \sim 0.7038$; $\varepsilon_{Nd} \sim +2$) and lack chemical evidence for crustal contamination (Ramos and Kay 1992; Gorring and Kay 2000). Thus, the source of their OIB-like isotopic signatures must reside in deeper, unsampled levels of the lithosphere or more likely in the asthenosphere. The only indirect evidence for enriched lithospheric components in this region comes from Pliocene main-plateau lavas from the northeastern sector of the Deseado Massif (Gorring and Kay 2000) and Pleistocene post-plateau lavas from the Meseta del Lago Buenos Aires (Hawkesworth et al. 1979; Stern et al. 1990; Ramos and Kay 1992). These lavas lack evidence for crustal contamination and have $^{87}Sr/^{86}Sr = 0.7046–0.7048$; $\varepsilon_{Nd} = +1–0$.

Significance of carbonatite metasomatism in Patagonia

The discovery of carbonatite metasomatism in southern Patagonia is significant because it occurs where extensive Neogene intraplate plateau magmas erupted in response to ridge–trench collision and the opening of asthenospheric slab windows between the subducting Nazca and Antarctic Plates (Gorring et al. 1997; Gorring and Kay 2000). Carbonatite metasomatism in this region is unexpected because young oceanic crust of the Nazca Plate was subducting during the mid-Miocene; thus adakitic metasomatism might be expected to dominate. In fact, some of the best examples of adakite lavas have erupted in the southern Patagonian backarc at Cerro Pampa (see Fig. 1) during this time (Kay et al. 1993). Furthermore, adakite metasomatized xenoliths have been reported farther south in the near Patagonian backarc (< 75 km behind the arc) at Cerro del Fraile (Kilian 1995), where young oceanic crust of the Antarctic Plate is currently being subducted (see Fig. 1). In this same region, Quaternary arc lavas of the Austral Volcanic Zone (AVZ) also have strong adakitic signatures (Stern and Kilian 1996). The data presented here do not lend strong support for the preservation of adakitic metasomatism in the far backarc of southern Patagonia. Stern et al. (1999) has also documented a lack of adakitic metasomatism in peridotite xenoliths from Pali–Aike (>200 km from the arc). We interpret this to reflect nearly complete overprinting of any prior adakite metasomatism by carbonatitic fluids/melts triggered by vigorous heating of the lithospheric mantle by upwelling slab window asthenosphere during Neogene plateau magmatism.

Carbonatite metasomatism has affected the southern Kamchatkan backarc mantle lithosphere at a distance of ~100 km behind the arc where relatively old oceanic lithosphere (~100 Ma) is subducting at present (Kepezhinskas and Defant 1996). They attribute this to melting of subducted carbonated basalt or carbonate-rich sediment. A similar style of carbonatite metasomatism was previously documented by McInnes and Cameron (1994) in subarc mantle xenoliths from the Tabar–Lihir–Tanga–Feni arc, Papua New Guinea. Here, the metasomatizing fluid is a SO_2–CO_2–H_2O-rich phonolitic melt. The low Ca/Al ratio (~1) of this melt and reactions that convert harzburgite or lherzolite to olivine-poor, phlogopite ± amphibole websterite or clinopyroxenite (McInnes and Cameron 1994) make it difficult to explain features of carbonatite metasomatism like those observed in Tanzanian, southeast Australian, or the Lote 17 xenoliths. This suggests that two types of carbonatite metasomatism may occur in active backarc regions. The first type is a SO_2–CO_2–H_2O-rich phonolitic melt derived from partial melting of carbonated oceanic crust or sediment in normal arc settings (e.g., McInnes and Cameron 1994; Kepezhinskas and Defant 1996). The second type is a CO_2-rich, sodic–dolomitic carbonatite melt derived from the asthenosphere or the continental lithosphere that occurs in intraplate (e.g., Hauri et al. 1993; Rudnick et al. 1993) and slab window settings, like southern Patagonia.

Conclusions

Major and trace element whole-rock and mineral separate data for spinel peridotite xenoliths from the Estancia Lote 17 locality indicate that carbonatite metasomatism has affected the continental lithosphere beneath southern Patagonia. Two distinct groups of peridotite xenoliths have been identified. Group 1 consists of a suite of fertile, hydrous peridotite xenoliths and Group 2 consists of infertile, anhydrous harzburgite xenoliths. Group 1 xenoliths are further divided into three subgroups based on the style and extent of carbonatite metasomatism.

Metasomatism of Group 1a xenoliths occurred by the open-system reaction of carbonatite melts with harz-

burgite and lherzolite to produce amphibole- or phlogopite-bearing wehrlites with high Ca/Al, Zr/Hf, Nb/La, and low Ti/Eu ratios. Chromatographic fractionation during transport through the lithosphere and precipitation of HFSE-, Rb-, Ba-rich phlogopite and amphibole in Group 1a xenoliths depleted the carbonatite melt in these elements. This fractionated carbonatite melt ultimately resulted in the metasomatism of Groups 1b and 1c hydrous xenoliths. Group 1b xenoliths have transitional characteristics that are attributed to an older H_2O-rich fluid and/or basaltic melt metasomatic event(s) that was overprinted by recent carbonatite metasomatism. Group 1c amphibole–apatite lherzolite xenoliths have strong HFSE depletion, strong enrichment of LREE, Th, and U, and "reacted" spinels that all indicate bulk addition of small amounts (~0.2%) of the fractionated carbonatite melt that metasomatized Group 1a and 1b xenoliths. CO_2-rich fluids liberated by metasomatic reactions that generated Group 1 xenoliths may have caused the cryptic metasomatism recognized in the Group 2 anhydrous harzburgites. Timing of the carbonatite metasomatism is constrained to be <25 Ma, based on the low $^{87}Sr/^{86}Sr$ and high $^{87}Rb/^{86}Sr$ ratios of Group 1a phlogopite separates. Thus, extensive Neogene plateau magmatism associated with the formation of asthenospheric slab windows is inferred as the primary thermal event that triggered carbonatite metasomatism in the Patagonian lithosphere. The lack of adakite metasomatism in the far Patagonian backarc suggests efficient mixing of adakitic slab melts in upwelling slab window asthenosphere or that adakite metasomatism only occurs immediately beneath the main-arc and near-backarc environment. Extremely variable trace element ratios and the depleted Sr–Nd isotope ratios ($^{87}Sr/^{86}Sr = 0.70294–0.70342$; $\varepsilon_{Nd} = +3.0–6.6$) of Lote 17 xenoliths indicate that the Patagonian mantle lithosphere is an unlikely primary source or an isotopically enriched contaminant for most Neogene Patagonian plateau lavas.

Acknowledgements This paper has benefited from discussions with R.W. Kay and W. McDonough and constructive reviews from C. Stern, P. Kepezhinskas, and R. Rudnick. The first author wishes to give special thanks to V.A. Ramos for his involvement in the project. This research was supported by NSF grant EAR-9219328, GSA grant 5156-93, the Cornell Chapter of Sigma Xi, and the Servicio Geológico Nacional de Argentina. This is a contribution to IGCP project 345, "Lithospheric Evolution of the Andean Continental Margin".

References

Bedini RM, Bodinier J-L (1999) Distribution of incompatible trace elements between the constituents of spinel peridotites xenoliths: ICP-MS data from the east African Rift. Geochim Cosmochim Acta 63: 3883–3900

Bodinier J-L, Merlet C, Bedini RM, Simien F, Remaidi M, Garrido CJ (1996) Distribution of niobium, tantalum, and other highly incompatible trace elements in the lithospheric mantle: the spinel paradox. Geochim Cosmochim Acta 60: 545–550

Cande SC, Leslie RB (1986) Late Cenozoic tectonics of the southern Chile Trench. J Geophys Res 91: 471–496

Chazot G, Menzies MA, Harte B (1996) Determination of partition coefficients between apatite, clinopyroxene, amphibole, and melt in natural spinel lherzolites from Yemen: implications for wet melting of the lithospheric mantle. Geochim Cosmochim Acta 60: 423–437

Cheatham MM, Sangrey WF, White WM (1993) Sources of error in external calibration ICP-MS analysis of geological samples and an improved non-linear drift correction. Spectrochim Acta 48B: E487–E506

Dautria JM, Dupuy C, Takherist D, Dostal J (1992) Carbonate metasomatism in the lithospheric mantle: peridotitic xenoliths from a melilitic district of the Sahara basin. Contrib Mineral Petrol 111: 37–52

Dawson JB (1984) Contrasting types of upper mantle metasomatism? In: Kornprobst J (ed) Kimberlites-II. Elsevier, Amsterdam, pp 289–294

Drummond MS, Defant MJ (1990) A model for trondhjemite–tonalite–dacite genesis and crustal growth via slab melting: Archean to modern comparisons. J Geophys Res 95: 21503–21521

Eggins SM, Rudnick RL, McDonough WF (1998) The composition of peridotites and their minerals: a laser-ablation ICP-MS study. Earth Planet Sci Lett 154: 53–71

Francis DM (1976) The origin of amphibole in lherzolite xenoliths from Nunivak Island, Alaska. J Petrol 17: 357–378

Frey FA, Green M (1978) The mineralogy, petrology, and origin of lherzolite inclusions in Victorian basanites. Geochim Cosmochim Acta 38: 1023–1059

Gorring ML, Kay SM (2000) Mantle processes and sources of Neogene slab window magmas from Southern Patagonia, Argentina. J Petrol (in press)

Gorring ML, Kay SM, Zeitler PK, Ramos VA, Rubiolo D, Fernandez MI, Panza JL (1997) Neogene Patagonian plateau lavas: continental magmas associated with ridge collision at the Chile Triple Junction. Tectonics 16: 1–17

Green DH, Wallace ME (1988) Mantle metasomatism by ephemeral carbonatite melts. Nature 336: 459–462

Green TH, Adams J, Sie SH (1992) Trace element partitioning between silicate minerals and carbonatite at 25 kbar and application to mantle metasomatism. Mineral Petrol 46: 179–184

Hamilton DL, Freestone IC, Dawson JB, Donaldson CH (1979) Origin of carbonatites by liquid immiscibility. Nature 279: 52–54

Hamilton DL, Bedson P, Esson J (1989) The behavior of trace elements in the evolution of carbonatites. In: Bell K (ed) Carbonatites: genesis and evolution. Unwin Hyman, London, pp 405–427

Hauri EH, Hart SR (1994) Constraints on melt migration from mantle plumes: a trace element study of peridotite xenoliths from Savai'I, western Samoa. J Geophys Res 99: 24301–24321

Hauri EH, Shimizu N, Dieu JJ, Hart SR (1993) Evidence for hotspot-related carbonatite metasomatism in the oceanic upper mantle. Nature 365: 221–227

Hawkesworth CJ, Norry MJ, Roddick JC, Baker PE, Francis PW, Thorpe RS (1979) $^{143}Nd/^{144}Nd$, $^{87}Sr/^{86}Sr$ and incompatible trace element variations in calc-alkaline andesitic and plateau lavas from South America. Earth Planet Sci Lett 42: 45–57

Hervé F (1988) Late Paleozoic subduction and accretion in southern Chile. Episodes 11: 183–188

Ionov DA, Hofmann AW (1995) Nb–Ta-rich mantle amphiboles and micas: implications for subduction-related metasomatic trace element fractionations. Earth Planet Sci Lett 131: 341–356

Ionov DA, Hofmann AW, Shimizu N (1994) Metasomatism-induced melting in mantle xenoliths from Mongolia. J Petrol 35: 753–785

Kay RW (1978) Aleutian magnesian andesites: melts from the subducted Pacific ocean crust. J Volcan Geotherm Res 4: 117–132

Kay SM, Maksaev V, Moscoso R, Mpodozis C, Nasi C (1987) Probing the evolving Andean lithosphere: mid–late Tertiary magmatism in Chile (29°–30.5°S) over the modern zone of subhorizontal subduction. J Geophys Res 92: 6173–6189

Kay SM, Ramos VA, Mpodozis C, Sruoga P (1989) Late Paleozoic to Jurassic silicic magmatism at the Gondwana margin: analogy to the middle Proterozoic in North America? Geology 17: 324–328

Kay SM, Ramos VA, Márquez M (1993) Evidence in Cerro Pampa volcanic rocks for slab-melting prior to ridge-collision in southern South America. J Geol 101: 703–714

Kelemen PB, Johnson KTM, Kinzler RJ, Irving AJ (1990) High-field strength element depletions in arc basalts due to mantle–magma interaction. Nature 345: 521–524

Kempton PD (1987) Mineralogic and geochemical evidence for differing styles of metaomatism in spinel lherzolites xenoliths: are they all analogues for enriched mantle source regions for basalts? In: Menzies M, Hawkesworth CJ (eds) Mantle metasomatism. Academic Press, London, pp 45–89

Kepezhinskas PK, Defant MJ (1996) Contrasting styles of mantle metasomatism above subduction zones: constraints from ultramafic xenoliths in Kamchatka. In: Bebout GE (ed) Subduction: top to bottom. AGU Geophys Monogr 96, pp 307–314

Kepezhinskas PK, Defant MJ, Drummond MS (1995) Na metasomatism in the island arc mantle by slab melt–peridotite interaction: evidence from mantle xenoliths in the North Kamchatka arc. J Petrol 36: 1250–1267

Kepezhinskas PK, Defant MJ, Drummond MS (1996) Progressive enrichment of island arc mantle by melt–peridotite interaction inferred from Kamchatka xenoliths. Geochim Cosmochim Acta 60: 1217–1229

Kilian R (1995) Interaction of tonalitic melts with mantle peridotite: evidence from a xenolith of the southern Andes. IUGG XXI General Assembly (Abstr), A468–469

Lindsley DH (1983) Pyroxene thermometry. Am Mineral 88: 477–493

Maaløe S, Aoki K (1977) The major element composition of the upper mantle estimated from the composition of lherzolites. Contrib Mineral Petrol 63: 161–173

Masuda A, Nakamura N, Tanaka T (1973) Fine structures of mutually normalized rare-earth patterns of chondrites. Geochim Cosmochim Acta 37: 239–248

Maury RC, Defant MJ, Joron J-L (1992) Metasomatism of the sub-arc mantle inferred from trace elements in Philippine xenoliths. Nature 360: 661–663

McDonough WF (1990) Constraints on the composition of the continental lithospheric mantle. Earth Planet Sci Lett 101: 1–18

McDonough WF, Stosch H-G, Ware N (1992) Distribution of titanium and the rare earth elements between peridotitic minerals. Contrib Mineral Petrol 110: 321–328

McInnes BIA, Cameron EM (1994) Carbonated, alkaline hybridizing melts from a sub-arc environment: mantle wedge samples from the Tabar–Lihir–Tanga–Feni arc, Papua New Guinea. Earth Planet Sci Lett 122: 125–141

Menzies MA, Rodgers N, Tindle A, Hawkesworth CJ (1987) Metasomatic and enrichment processes in lithospheric peridotites, and effect of asthenosphere–lithosphere interaction. In: Menzies M, Hawkesworth CJ (eds) Mantle metasomatism. Academic Press, London, pp 313–361

Muñoz JB (1981) Inclusions ultramaficas del manto superior en Meseta las Vizcachas, ultima esperanza, Magallanes, Chile. Rev Geol Chile 13–14: 63–78

Navon O, Stolper E (1987) Geochemical consequences of melt percolation: the upper mantle chromatographic column. J Geol 95: 285–305

Niemeyer H (1978) Nodulos maficos y ultramaficos en basaltos alcalinos de la Meseta Buenos Aires, Lago General Carrera, Provincia de Aysen, Chile. Assoc Geol Argent Rev 33: 63–75

O'Reilly SY, Griffin WL (1988) Mantle metasomatism beneath western Victoria, Australia, I. metasomatic processes in Cr-diopside lherzolites. Geochim Cosmochim Acta 52: 433–447

O'Reilly SY, Zhang M (1995) Geochemical characteristics of lava-field basalts from eastern Australia and inferred sources: connections with the subcontinental lithospheric mantle? Contrib Mineral Petrol 121: 148–170

O'Reilly SY, Griffin WL, Ryan CG (1991) Residence of trace elements in metasomatized spinel lherzolite xenoliths: a proton-microprobe study. Contrib Mineral Petrol 109: 98–113

Pankhurst RJ, Rapela CR (1995) Production of Jurassic rhyolite by anatexis of the lower crust of Patagonia. Earth Planet Sci Lett 134: 23–36

Pankhurst RJ, Hervé F, Rapela CR (1994) Sm–Nd evidence for the Grenvillian provenance of the metasedimentary basement of southern Chile and west Antarctica. Actas VII Congr Geol Chileno 2: 1414–1418

Panza JL, Nullo FE (1994) Mapa geológico de la provincia de Santa Cruz, República de Argentina, 1:750000. Servicio Geológico de Argentina, Buenos Aires

Ramos VA (1988) Late Proterozoic–Early Paleozoic of South America- a collisional history. Episodes 11: 168–174

Ramos VA, Kay SM (1992) Southern Patagonian plateau basalts and deformation: backarc testimony of ridge collision. Tectonophysics 205: 261–282

Ramos VA, Niemeyer H, Skarmeta J, Muñoz J (1982) Magmatic evolution of the Austral Patgaonian Andes. Earth Sci Rev 18: 411–443

Rampone E, Botazzi P, Ottolini L (1991) Complementary Ti and Zr anomalies in orthopyroxene and clinopyroxene from mantle peridotites. Nature 354: 518–520

Rudnick RL, McDonough WF, Chappell BW (1993) Carbonatite metasomatism in the northern Tanzanian mantle: petrographic and geochemical characteristics. Earth Planet Sci Lett 114: 463–475

Schiano P, Clocchiatti R, Shimizu N, Maury RC, Jochum KP, Hofmann AW (1995) Hydrous, silica-rich melts in the sub-arc mantle and their relationship with erupted arc lavas. Nature 377: 595–600

Stern CR, Kilian R (1996) Role of the subducted slab, mantle wedge, and continental crust in the generation of adakites from the Andean Austral Volcanic Zone. Contrib Mineral Petrol 123: 263–281

Stern CR, Saul S, Skewes MA, Futa K (1989) Garnet peridotite xenoliths from the Pali-Aike basalts of southernmost South America. In: Ross J (ed) Kimberlites and related rocks, vol 2, Proc 4th Int Kimberlite Conf, Geol Soc Aust Spec Pub 14, pp 735–744

Stern CR, Frey FA, Futa K, Zartman RE, Peng Z, Kyser TK (1990) Trace element and Sr, Nd, Pb, and O isotopic composition of Pliocene and Quaternary alkali basalts of the Patagonian Plateau lavas of southernmost South America. Contrib Mineral Petrol 104: 294–308

Stern CR, Kilian R, Olker B, Hauri EH, Kyser TK (1999) Evidence from mantle xenoliths for relatively thin (< 100 km) continental lithosphere below the Phanerozoic crust of southernmost South America. Lithos 48: 217–235

Sun M, Kerrich R (1995) Rare earth element and high field strength element characteristics of whole rocks and mineral separates of ultramafic nodules in Cenozoic volcanic vents of southeasten British Columbia, Canada. Geochim Cosmochim Acta 59: 4863–4879

Sun SS, McDonough WF (1989) Chemical and isotopic systematics of oceanic basalts; implications for mantle composition and processes. In: Saunders AD, Norry MJ (eds) Magmatism in the ocean basins. Geol Soc Spec Publ 42: 313–345

Sweeney RJ, Green DH, Sie SH (1992) Trace and minor element partitioning between garnet and amphibole and carbonatitic melt. Earth Planet Sci Lett 113: 1–14

Tatsumoto M, Basu AR, Wankang H, Junwen W, Guanghong X (1992) Sr, Nd, and Pb isotopes of ultramafic xenoliths in volcanic rocks of Eastern China: enriched components EMI and EMII in subcontinental lithosphere. Earth Planet Sci Lett 113: 107–128

Thibault Y, Edgar AD, Lloyd FE (1992) Experimental investigation of melts from a carbonated phlogopite lherzolite: implications for metasomatism in the continental lithospheric mantle. Am Mineral 77: 784–794

Wallace ME, Green DH (1988) An experimental determination of primary carbonatite magma composition. Nature 335: 343–346
Wasserburg GJ, Jacobsen SB, DePaulo DJ, McCulloch MT, Wen T (1981) Precise determination of Sm/Nd ratios, Sm and Nd isotopic abundances in standard solutions. Geochim Cosmochim Acta 45: 2311–2323
Webb SAC, Wood BJ (1986) Spinel–pyroxene–garnet relationships and their dependence on Cr/Al ratio. Contrib Mineral Petrol 92: 471–480
Wells PRA (1977) Pyroxene thermometry in simple and complex systems. Contrib Mineral Petrol 62: 129–139
White WM, Duncan RA (1996) Geochemistry and geochronology of the Society Islands: new evidence for deep mantle recycling. In: Basu A, Hart S (eds) Earth processes: reading the isotopic code. AGU Geophys Monogr 95, pp 183–206
Wiechert U, Ionov DA, Wedepohl KH (1997) Spinel peridotite xenoliths from the Atsagin–Dush volcano, Dariganga lavas plateau, Mongolia: a record of partial melting and cryptic metasomatism in the upper mantle. Contrib Mineral Petrol 126: 345–364
Wilshire HG, Meyer CE, Nakata JK, Calk LC, Shervais JW, Nelson JE, Schwarzmann EC (1988) Mafic and ultramafic xenoliths from volcanic rocks of the western United States. US Geol Surv Prof Pap 1443
Wooley AR, Kempe DRC (1989) Carbonatites: nomenclature, average chemical compositions, and element distribution. In: Bell K (ed) Carbonatites: genesis and evolution. Unwin Hyman, London, pp 1–14
Yaxley GM, Green DH (1996) Experimental reconstruction of sodic dolomitic carbonatite melts in from metasomatised lithosphere. Contrib Mineral Petrol 124: 359–369
Yaxley GM, Crawford AJ, Green DH (1991) Evidence for carbonatite metasomatism in spinel peridotite xenoliths from western Victoria, Australia. Earth Planet Sci Lett 107: 305–317
Yaxley GM, Kamenetsky V, Green DH, Falloon TJ (1997) Glasses in mantle xenoliths from western Victoria, Australia, and their relevance to mantle processes. Earth Planet Sci Lett 148: 433–446
Zartman RE, Futa K, Peng ZC (1991) A comparison of Sr–Nd–Pb isotopes in young and old continental lithospheric mantle: Patagonia and eastern China. Aust J Earth Sci 38: 545–557
Zindler A, Hart SR (1986) Chemical geodynamics. Annu Rev Earth Planet Sci 14: 493–571